NASA TECHNICAL NOTE

NASA TN D-4041

NASA TN D-4041

ATTACHED AND SEPARATED BOUNDARY LAYERS ON HIGHLY COOLED, ABLATING AND NONABLATING MODELS AT M = 13.8

by Donald M. Kuehn and Daryl J. Monson

Ames Research Center
Moffett Field, Calif.

NATIONAL AERONAUTICS AND SPACE ADMINISTRATION • WASHINGTON, D. C. • JUNE 1967

NASA TN D-4041

ATTACHED AND SEPARATED BOUNDARY LAYERS ON HIGHLY COOLED, ABLATING AND NONABLATING MODELS AT M = 13.8

By Donald M. Kuehn and Daryl J. Monson

Ames Research Center
Moffett Field, Calif.

NATIONAL AERONAUTICS AND SPACE ADMINISTRATION

For sale by the Clearinghouse for Federal Scientific and Technical Information
Springfield, Virginia 22151 – CFSTI price $3.00

TABLE OF CONTENTS

ATTACHED AND SEPARATED BOUNDARY LAYERS ON HIGHLY COOLED, ABLATING AND NONABLATING MODELS AT M = 13.8

By Donald M. Kuehn and Daryl J. Monson

Ames Research Center

SUMMARY

Separated and attached flows were studied on ablating and on nonablating models at M = 13.8. Two types of axisymmetric models were tested: 1) cylinder-flare models with conical and hemispherical noses, and 2) blunt-faced base-flow models. The boundary layers on these highly cooled models (i.e., $T_w \ll T_{st}$) were generally laminar, but in a few cases appeared to have been transitional. The Reynolds numbers were very low; thus the viscous layers were extremely thick. Nonablating models were used to study effects of Reynolds number and model geometry on separation and to examine incipient separation conditions at low Reynolds numbers. Effects of ablation were determined by comparison of experimental data from ablating and nonablating models. The flows were studied with the aid of pressure distributions, surface oil accumulations and streaks, burn patterns, and photographs of the flow about the models.

The two most significant results for the nonablating models were associated directly with the very low Reynolds number of the tests. Large turning angles with no separation were observed for the thick, highly cooled laminar boundary layers. The present experiments show, as do some previously published data, that as Reynolds number decreases the extent of laminar separation also decreases. At the lower Reynolds number, the flow was completely attached to a 45° compression corner. The second phenomenon associated with this low Reynolds number was the merging of the viscous layer and shock wave. This is believed to have caused the decrease in surface pressure ratio for the attached flows as Reynolds number was decreased. (For thinner boundary layers where the growth of displacement thickness predominates, a decrease in Reynolds number causes surface pressures to increase.)

Ablation influenced surface pressures and boundary-layer transition in some cases, but generally had very little influence on the extent of laminar separation. Photographs showed that the ablation gases deeply penetrated the flow fields about the test models. Nose ablation had no influence on the extent of laminar separation, but flare ablation increased the extent of separation slightly. Surface pressures were increased by nose ablation in regions of attached flow as a result of a growth in displacement thickness beginning near the nose of the model. Flare ablation caused a further increase in pressures as a result of an increase in extent of separation and a thickened shock layer. On the cone-cylinder-flare models at high Reynolds number, ablation appeared to have reduced the transition Reynolds number.

INTRODUCTION

Predicting boundary-layer separation on entry vehicles continues to be a problem because theoretical methods are generally inadequate, and appropriate experimental data are limited. Some experimental results for axisymmetric models describe the dependence of incipient laminar separation upon some of the important variables, such as Mach number, Reynolds number, and boundary-layer cooling (see, e.g., refs. 1, 2). One variable, not yet investigated, is the influence on separation of mass added to the boundary layer by ablating surfaces.

The purpose of this investigation was to determine experimentally the gross effects of ablation on laminar boundary-layer separation by comparing the flow about ablating models with that for nonablating models. Since these experiments are intended to be useful in predicting separation, information on the attached boundary layer ahead of separation is also given (some of the present experimental results are included in ref. 3). Two classes of models were studied: cylinder-flare models with conical and hemispherical noses; and blunt-faced base flow models with converging afterbodies (similar to the Mercury or Gemini shape) followed by a cylinder to which the boundary layer can attach. Various flare and base angles were tested in order to span the conditions from attached flow to separated flow. The models were tested at zero angle of attack in a hypersonic test stream of low-density, arc-heated air. Three ablating materials were used to provide a variation of ablation characteristics.

NOTATION

A^* nozzle throat area

A area of nozzle cross section downstream of the throat

d diameter of the cylindrical portion of the models

D maximum diameter of the flares and bases

h_{st} stagnation enthalpy

$\dot{m}$ total mass loss rate of ablating material (includes melt and gas)

$\dot{m}_\infty$ free-stream mass flow rate over an area of $\pi d^2/4$ for the cylinder-flare models and $\pi D^2/4$ for the base models

M_e Mach number at the boundary-layer edge

M_∞	Mach number in the free stream
p	static pressure on the cylinder (without orifice wedge)
p_n	static pressure along the nozzle center line
p_{t_1}	arc-chamber pressure
p_{t_2}	pitot pressure at the location of the model nose in the test stream
p_w	static pressure on the cylinder with orifice wedge in place
$\dot{q}_{st}$	stagnation heating rate
$Re_{e,d}$	Reynolds number based on properties at boundary-layer edge and on cylinder diameter
R_b	radius of hemispherical nose
$Re_{\infty,d}$, $Re_{\infty,D}$	Reynolds numbers based on free-stream properties and on model diameters
T_w	wall temperature of the model
T_{st}	stagnation temperature
x	distance along the cylinder measured from the nose-cylinder juncture, or the base-cylinder juncture
y	distance normal to the cylinder measured from the model axis
δ	boundary-layer velocity thickness (velocity = 0.99 of the inviscid-flow velocity)
δ^*	boundary-layer displacement thickness
θ	angle of the flares and bases
Φ	boundary-layer momentum thickness

EQUIPMENT AND PROCEDURES

Test Facility

The experiments were run in arc-heated air at a Mach number of 13.8. The arc heater (shown in fig. 1) is a commercially available Linde N-4000 unit, which is essentially a scaled up version of the Linde Model 124 heater (ref. 4). The models were tested in the free-jet discharge from the 8° half-angle nozzle. Figure 2 gives the general layout and dimensions of the facility.

Test Conditions

The two reservoir conditions chosen gave a maximum range of Reynolds number. The upper limit was dictated by maximum permissible reservoir pressure, and the lower limit by boundary-layer growth that reduced the size of test core. Values of stagnation enthalpy varied as the reservoir pressure was changed. The nominal test conditions are listed in table I. The values of pressure, heating rate, and enthalpy are averages of the values for all runs at a particular condition and the deviations from these averages are the maximum due to a combination of instrument and tunnel repeatability. The other properties were determined from a nozzle-flow calculation using average stagnation properties. Where properties varied longitudinally as a result of conical nozzle flow, the values are those at the average location of the model nose. (The variation in the location of the model nose in the test stream is discussed in following sections.)

The stagnation enthalpy on the center line of the nozzle was calculated by means of the theory of Fay and Riddell (ref. 5). Experimental measurements used in this calculation were pitot pressure and the time rate of change of the temperature of a thermally insulated copper slug (from which heating rate was derived) at the stagnation point of a hemispherical-nosed calorimeter. The temperature was measured with a Chromel-Alumel thermocouple fastened to the back of the slug. Reference 5 was used in conjuction with the air transport properties of Hansen (ref. 6), stagnation-point velocity gradients from a correlation by Inouye (ref. 7), and vorticity interaction corrections of Cheng (ref. 8). In addition, a frozen boundary layer with a fully catalytic wall was assumed.

An alternate calculation of enthalpy was made using the charts of reference 9 for the sonic-flow method. On the average, the enthalpy from the sonic-flow method was higher than that obtained from the calorimeter measurements by 22 percent at the high Reynolds number condition and 14 percent at the low Reynolds number condition. These differences are reasonable in view of the approximations in the theories and possible experimental errors. The values of heating rate obtained from calorimeter measurements, shown in table I, are believed to be more appropriate to the present tests because they represent measurements taken at the model location, whereas the enthalpy from the sonic flow method is an average value over the nozzle cross section at the throat.

A computer program for nonequilibrium nozzle flow (ref. 10), together with measured stagnation properties, was used to calculate additional required stream properties. The values of Mach number and Reynolds number, shown in table I, correspond to the effective value of A/A^* that was determined from pitot-tube measurements. The theoretical center line static pressure in the nozzle is shown in figures 3(a) and 3(b) for the high and low Reynolds number conditions. The pressures are compared with the limiting cases of equilibrium flow and flow frozen in the arc chamber (frozen in vibration and dissociation only). Although it is not obvious from figure 3, the calculations indicated that the test stream became frozen a short distance downstream of the nozzle throat. Other stream properties show a similar state of the gas.

The temperature ratios given in table I were calculated. The lower value at each condition corresponds to the initial temperature of the model wall (approx. 290° K); the larger value corresponds to the maximum estimated final temperature of a nonablating model (approx. 400° K). The stagnation temperature was obtained from the results of the nonequilibrium nozzle-flow calculation and the perfect-gas relationship for temperature rise across a normal shock.

Surveys of pitot pressure and stagnation enthalpy in the test stream showed a core of nearly constant stream properties that was larger than any of the models for both test conditions (see fig. 4). The survey also revealed a center-line axial gradient in p_{t_2}/p_{t_1} of about 4.7×10^{-6}/cm at both conditions, which was not significant to these tests.

Models

The model shapes and dimensions are shown in figure 5. All model configurations were tested as nonablating models and as ablating models.

The nonablating models were machined from copper and aluminum. In the model construction the volume of material retained was as large as possible to provide a heat sink so that the model temperature would remain low relative to the stagnation temperature. Noses, flares (or bases) and cylindrical portions of the models were separate and interchangeable. A cylindrical section contained eight static-pressure orifices (diam. = 0.063d) spiralled around the circumference at intervals of 45° and spaced longitudinally at a distance of 0.15d. To obtain data at various longitudinal locations, cylindrical extensions of different length were inserted between the cylindrical section containing the orifices and the nose section. The longitudinal location of the nose in the test stream varied by about 5d as the length of extension was changed.

Models were also tested with ablating surfaces as shown by the shaded areas in figure 5. The nonablating portion of these models was described in the previous paragraph. Conical and hemispherical ablating noses were machined from Teflon, Delrin, and phenolic nylon. The noses on the base model were made of Teflon and Delrin only. Ablating flares (θ = 45°) of all

three materials were made for the hemispherical-nosed model. This model was tested with an ablating nose only, and with an ablating nose and flare of the same material.

Pressure Measurement

The pressures measured were static pressure on the cylindrical portion of all models, pitot pressure at the nose of the nonablating blunt models, and arc-chamber pressure. The measured static pressures were not corrected for the longitudinal stream gradient, caused by the conical nozzle, or for possible orifice effects caused by the low pressure and high temperature. These effects were not believed to be significant, primarily because pressure distributions were used on a comparative basis rather than on an absolute basis -- all data at a given test condition for a specified model should be subject to nearly the same corrections. The effect on the pressure distribution of the variation in Mach number at the nose of the model (resulting from a variation in nose position in the test stream) was negligible since static pressure was referred to measured pitot pressure. Pitot pressures for ablating models and conical-nosed models were obtained from a ratio of p_{t_2}/p_{t_1} that was established from runs during which p_{t_2} was measured. Although p_{t_2} may not have the same significance for the conical-nosed model as for the blunt-nosed models, this reference was used for all pressure data.

The pressure system for measuring static pressures was accurate to within about 5 percent at the lowest pressures (30 μ), and to within 1 percent at the highest pressures (1000 μ). Capacitance-type pressure transducers (Datametrics Barocel) were used. The length of connecting tubing (inside diam. = 0.12d) between orifice and transducer was about 2 meters. At low pressures the lag time was about 5 seconds, but this presented no problem because the run times were from 20 to 40 seconds. Considerable attention was given to the problem of outgassing (this is discussed later). Tubing and connectors were all metal, except for O-rings in the connectors. The entire pressure system was continuously outgassed, except during the runs (outgassing pressure was about 1 μ).

Pitot pressure and tunnel stagnation pressure are accurate to better than 1 percent, with the exception of pitot pressure at the low Reynolds number, where the accuracy is probably no better than 2 percent. Details of these pressure systems are not given because the measurement of these higher pressures does not involve special problems as was the case for the low pressures.

Test Methods

General procedures.- Since the process of starting the arc facility often took nearly a minute, it was necessary to protect the models from the hot stream during this time. This was done in two ways. For most tests, a

shield was inserted into the stream ahead of the model during the starting process and retracted when flow was established. This system was used satisfactorily for the oil flow studies on the cylinder-flare models and in all tests when pressures were measured. (Pressure models had to be fixed in the test stream because of the rigid metal tubing that connected model and transducers.) The shield was not satisfactory for protecting the oil on the base-flow model, so it was necessary to retract the model from the stream during the starting process and insert it when the flow was established. (This was possible only when the rigid pressure tubing was disconnected.)

Proper techniques are essential for measuring low pressures in order to eliminate the deleterious effects of outgassing. A particular problem associated with the open-jet arc facility is that in order to minimize the length of connecting tubing, the pressure transducers are located inside the vacuum tank. It is difficult to outgas this system up to the time of pressure measurement unless remotely controlled valves are located in the pressure line close to the orifice. The following procedures were adopted because the models were too small to house eight remotely controlled valves. With tape over the orifices, the entire pressure system was continuously outgassed during nontesting time. With an outgassed system, the transducers were calibrated each day (often several times a day) to provide a continuous check on performance and reliability. Prerun preparation required that the tape be removed from the orifices before closing and evacuating the tank; thus a portion of the connecting tubing was at atmospheric pressure for about 5 minutes. (Remotely controlled valves between the orifice and the transducer permitted continuous outgassing of the transducers.) During this 5-minute period, the connecting tubing exposed to atmospheric pressure reabsorbed enough air to require another period of outgassing. This was done at a tank pressure of about 20 μ for 1/2 hour when minimum pressures of 30 μ were to be measured. The remotely controlled valves, which permitted outgassing of the transducers at about 1 μ, were opened after the facility was started and the protective shield removed and were again closed before the facility was shut down. (This procedure also minimized possibilities of contaminating the transducers with impurities from the arc stream.) During the run, pressure was recorded continuously. Since only 8 pressure points were obtained in one run, it was often necessary to make more than one run to complete one pressure distribution -- ample overlap was allowed for each segment of the pressure distribution and many repeat runs were made to evaluate repeatability.

Enthalpy was determined from measurements that were made at the beginning of each run and occasionally at the end of the run also. After the test condition was established, but before the model protective shield was retracted (or model inserted), the calorimeter was put into the stream on the longitudinal center line. The calorimeter was then retracted and the run proceeded. Enthalpy was believed to remain constant during the run (this was shown to be true where two measurements were taken).

Flow visualization played an important role in these experiments, and a photographic record of all visual observations was necessary. Ektachrome film provided excellent contrast of the various colors on the models and in

the flow fields. Several cameras in different positions provided a continuous record of the flow field about the models during runs, and of the oil patterns and condition of the model surface both during and after the runs.

Techniques for detecting separation and reattachment.- Various techniques were used to locate flow separation and reattachment. The usefulness of a particular technique depended upon the model and test condition; thus different combinations of techniques were used for the two types of models.

Separated or attached flow on the cylinder-flare models was indicated by flow-field photographs, oil accumulations and streaks (diffusion pump oil with red dye), and burn patterns on painted and ablating flares. Photographs of the glow about the models were useful in determining the approximate extent of separation (from the wedge of separated flow ahead of the flare as illustrated in fig. 6(a)), and in determining the thickness of the layer that contained the ablation gases (figs. 6(a) and 6(b)). To locate separation, or to indicate attached flow, drops of oil were put on the upper surface of the cylinder only. An accumulation of oil marked flow separation (figs. 6(c) and 6(d)); oil streaks downstream along the cylinder and up the flare (fig. 6(e)) indicated attached flow. Reattachment was located by the demarcation between burned and unburned regions on an ablating flare (fig. 6(f)) and on a white painted flare (fig. 6(g)). Reference marks on this flare were at intervals of 0.33d along the surface. Flow direction on the flare, which aided in locating flow reattachment, was detected by the patterns formed around small obstructions that had been cemented to the painted surface (fig. 6(g)). The surface downstream of the obstruction at 1.33d (burned off late in the run) was sheltered from the hot, reattaching boundary layer, indicating attached flow at that point. The surface upstream of the obstruction at 1.0d was sheltered from the hot gas, indicating reverse flow in a separated region. Reattachment could generally be narrowed down to a region about 0.3d long. (The center of this region is indicated in figures where the location of reattachment is specified.)

Separated or attached flow on the base models was detected by oil accumulations, oil streaks, and orifice wedges. Before nozzle flow was established, oil bubbled from holes in the model surface and ran around the model normal to the longitudinal axis (the vertical oil-flow marks in figs. 6(h), 6(i), and 6(j)). During a run the oil flowed along the model. Accumulation of this oil indicated the separation point (fig. 6(h)). Surface-flow direction in attached and separated regions was determined by the direction of the oil streaks (figs. 6(h), 6(i), and 6(j)). The streaks are very obvious in regions of high density. To observe the flow of oil in regions of low density and to observe the flow of oil that bubbled out of the holes as the run proceeded, it was necessary to study many photographs taken during the run. Figures 6(i) and 6(j) show the development of oil streaks in one run. Flow reattachment was also located with orifice wedges. Small-angle wedges (about 1 orifice diameter high, 1.5 diameters wide, and 3 diameters long) were cemented to the model upstream of the orifice, with the blunt base at the edge of the orifice (a sketch is shown in fig. 11). For attached flow, the orifice pressure with the wedge was less than that without the wedge; for separated flow the reverse was true. Again, the reattachment region was narrowed down to a length of about 0.3d.

Ablation Materials and Characteristics

The ablation materials used were Teflon (TFE), Delrin, and high density phenolic nylon (50% phenolic, 50% nylon; density of 1.19 g/cm^3). These three materials were chosen to give large rates of ablation, and ablation gases with different properties. The rates are the actual weight loss (as opposed to weight loss per unit area) due to both melt and gas, divided by the total time the material was exposed to the test stream. The ratio of gas to melt is not known. Ratios of the total mass loss rate to free-stream mass flow rate given in the figures are averages of all the runs for a particular material, configuration, and test condition. Scatter about these averages at the high Reynolds number was 20 percent for the hemispherical and conical noses, and less than 10 percent for the flares and the noses on the base flow models, and at the low Reynolds number was less than 10 percent for all shapes.

The Teflon pyrolized with no noticeable flow of melt. The ablation rates for this material were the lowest, but the rate apparently reflects the amount of gas injection into the boundary layer (as opposed to the other two materials where some of the weight loss was in liquid). The surface of the Teflon always remained smooth, and the shape of the ablating surfaces changed only small amounts. Time to ablate after exposure to the test stream was about 1 to 2 seconds. Further details on Teflon may be found in references 11 and 12.

The ablation rates for Delrin were relatively high but, depending upon test condition and model shape, a significant portion of the weight loss was in melt. Generally speaking, the amount of melt was sizable at the high Reynolds number condition and small at the low Reynolds number condition, possibly in a ratio of 5 or 10 to 1 (from this trend it might be expected that at some conditions no melt would occur). Models with Delrin noses tested at both conditions are shown in figure 7 (the melt curled up and pulled away from the surface due to cooling after the run). At the high Reynolds number, considerable melt dripped off the model during the run so only a portion of the total melt remained on the model after the run (fig. 7(a)); at the low Reynolds number, all the melt stayed on the model (fig. 7(b)). The Delrin surface was covered with small bubbles from the beginning of ablation (about 3 to 5 sec required to begin ablation) to the end of the run. The large ablation rates resulted in sizable changes in nose shapes (see section on Time Dependent Pressures for further discussion on the change of nose shape).

The phenolic nylon also gave fairly large ablation rates, but as with the Delrin, a portion of this weight loss was also in melt. The volume of melt was, however, judged to be much less than for the Delrin. Early in the run a bubbly melt appeared on the surface of the phenolic nylon; as the run progressed, the melt flowed back over the nose. Later in the run the surface charred where the heating rates were sufficiently high. The char was slightly rough and pitted, but would be considered smooth relative to the Delrin. The phenolic nylon began to ablate after about 3 to 5 seconds exposure to the test stream. The ablation of phenolic nylon is discussed in greater detail in references 12 to 14.

RESULTS AND DISCUSSION

Description of the Local-Flow Test Environment

The description of the local-flow properties ahead of separation is primarily theoretical and applies only to the nonablating models, but some experimental observations for both ablating and nonablating models are included.

State of equilibration.- The inviscid flow about all the test models is believed to have been out of equilibrium at both test conditions. Theoretical calculations, by the method of reference 15, indicated that the energies of vibration and dissociation in the stagnation region of the hemispherical nose were not significantly different from the free-stream values for both test conditions; that is, the flow across the bow shock was frozen in vibration and dissociation (the test stream was also frozen). Further downstream, the resident time decreases (velocity increases) and reaction time increases (pressure and temperature decrease) which favors the continuance of frozen flow over the entire model.

The state of equilibration over the base model and the conical-nosed model was not calculated, but from the results for the hemisphere it appears likely that the flow over these two models was also near frozen. The conditions over the face of the base model were slightly more favorable for relaxation than were the conditions for the hemisphere, but the rapid expansion at the shoulder followed by the region of low pressure and temperature would likely result in frozen flow over the base. The conditions over the cone-cylinder models favored frozen flow even more so than for the hemisphere-cylinder models because the weaker bow shock on the cone did not alter free-stream properties as much as the stronger shock on the hemispherical-nosed model.

Classification of stagnation viscous flow.- The extent to which viscosity might be important to the flow about a blunt-nosed vehicle is indicated by the viscous flow in the stagnation region. Probstein and Kemp (ref. 16) describe several flow regimes in the order of decreasing Reynolds number (three of these are of immediate interest). The first is the vorticity interaction regime, characterized by a thin shock wave, an inviscid layer, and a boundary layer. In the second regime the viscous layer fills the entire shock layer, but the shock remains thin (ref. 17 indicates that the shock does not remain thin). In the third regime, the viscous layer merges with a thickened shock wave; this is the incipient merged-layer regime. The shock layer remains a continuum.

On the basis of calculations by the method of reference 16, large viscous effects can be expected on some of the present models. The flow in the stagnation region of the hemispherical-nosed model at the lower Reynolds number was in the viscous layer regime. At the higher Reynolds number, the stagnation region flow was close to the upper limit of the vorticity interaction regime. The flow in the stagnation region of the base models was above the vorticity interaction regime, where viscous effects are expected

to be small. The strong expansion at the shoulder, however, caused the local Reynolds number to become so low that the base flow was probably highly viscous, especially at the lower Reynolds number where the stagnation region flow was not far above the vorticity interaction regime.

Location of transition.- The boundary layers in this investigation are believed to have been laminar, except on some of the conical-nosed models at the high Reynolds number condition (the transitional flows are discussed later). Although transition has not been located directly, the following evidence indicates laminar flow: 1) The length Reynolds numbers were very low. The highest in the investigation was for the conical-nosed model (Re_∞, length $\cong$ 78,000). Transition is believed to have been located slightly ahead of the flare at this condition when an extremely rough, nonablating nose or an ablating nose was used, but there was no evidence of transition on the model with a smooth nose. (It is possible, however, that transition might have been in the reattachment zone with the smooth nose.) For all other combinations of model and test condition, the length Reynolds number (based upon local-flow conditions) was, at least, about an order of magnitude less than the value quoted above. It seems reasonable, therefore, to believe that transition did not occur on the models with the lower length Reynolds numbers. 2) The boundary layers behaved like laminar boundary layers, not like transitional boundary layers. In all cases, the extent of separation decreased as Reynolds number was decreased (this will be shown in sections to follow). This behavior is characteristic of a laminar boundary layer -- the presence of transition would have been easily recognized by an opposite trend in the extent of separation (see discussion of the influence of Reynolds number). The trend in extent of separation with Reynolds number is the same for laminar and turbulent boundary layers, but because of the low Reynolds numbers of these experiments, the only concern here is whether the boundary layers were completely laminar or were transitional.

Attached viscous flow over the nonablating models.- Theoretical calculations were made by the method of reference 18 to estimate the viscous attached frozen flow about the hemisphere-cylinder and the cone-cylinder at both test conditions (no method was available for the base model). The method of reference 19 was used to estimate the inviscid flow field. Boundary-layer edge properties, rather than wall properties, were used in calculating the viscous flow because using wall properties gave unrealistic results in some cases (i.e., a boundary layer that grew outside of the experimental shock wave). A first estimate of the edge properties was obtained from the inviscid flow field by assuming a boundary-layer thickness; iterations were made as necessary. (The inviscid flow outside of the boundary layer was assumed to be unaffected by the presence of a boundary layer; this, of course, is not true.) The results to be shown indicate that the boundary layers fill a large portion of the shock layers at both test conditions. In the application of the methods of references 18 and 19 to such highly viscous flows, two limitations are immediately apparent, namely: 1) the method of reference 18 is for thin boundary layers, thus the assumptions on which the theory is based are not valid for a very thick layer in a nonuniform flow field, and 2) the boundary-layer edge properties obtained from the inviscid-flow calculation are questionable for such highly viscous

flows. Obviously, these limitations cast doubt on the results of the calculations (especially at the lower Reynolds number), but since a more suitable method is not available, references 18 and 19 were used to obtain an approximation of these highly viscous flows.

The boundary-layer velocity thickness, momentum thickness, and displacement thickness are shown in figures 8 and 9 for the hemisphere-cylinder and the cone-cylinder models at both test conditions. These thicknesses are given because previous experimental investigations have indicated that a Reynolds number based upon some characteristic dimension of the boundary layer is important to separation (in refs. 1 and 20, velocity thickness was used as the characteristic dimension, but displacement or momentum thickness might be more appropriate). The theoretical viscous layers were apparently very thick on the nonablating models; in some cases the viscous layer appears to merge with the shock wave. This is consistent with observations of the experimental data that showed the layers containing the ablation gases were also very thick, in some cases these ablation gases appear to merge with the shock wave, for example, figures 6(a), 6(b), 6(e), 8, and 9 (quantitative comparison of the thickness of the layers that contained ablation gases and the theoretical boundary-layer thickness for nonablating models is not intended).

The values of Mach number and Reynolds number at the edge of the estimated boundary layers (at the station where the flare began) are also shown in figures 8 and 9. These values were obtained from the inviscid flow calculation that did not account for viscid-inviscid flow interaction. Edge properties are significant to the development of the attached boundary layer (see ref. 18 and the preceding discussion) and are believed to be significant to the occurrence of separation (e.g., refs. 1 and 20). It is not known, however, whether the edge properties for a very thick boundary layer in a nonuniform flow field have the same significance to separation as seems to be the case when the boundary layer is thin.

Influence of Reynolds Number on the Extent of Laminar Separation

Published data appear to show opposite effects of Reynolds number on the extent of laminar separation. It was shown in reference 21 that the extent of separation increased as Reynolds number was decreased, and it was further pointed out that this trend was opposite to that which had previously been shown in reference 1 (the trend of extent of separation as affected by other variables discussed in ref. 21, e.g., Mach number, was also opposite to that shown in ref. 1). This matter was discussed by Gray with no definite conclusion. The following discussion is intended to show that the apparent opposite trends can be explained simply by recognizing the fundamental importance of the definitions of laminar and transitional separations. As defined in reference 22, transition is downstream of reattachment for a laminar separation and between separation and reattachment for a transitional separation. These definitions were not arbitrary, but instead were based upon marked changes in the observed characteristics of separated flows for different locations of transition.

The variation in extent of laminar and transitional separations with Reynolds number is shown in references 1 and 22, respectively. Transition was definitely located in both of these investigations with the aid of shadowgraphs; thus these boundary layers properly correspond to the definitions in reference 22. The behavior of the separations changed markedly as transition passed through the reattachment zone. For laminar separations (ref. 1), the extent of separation decreased as Reynolds number was decreased. Typical behavior of transitional separations is shown in reference 22 to be opposite to that for a laminar boundary layer (this is, of course, because a decrease in Reynolds number causes the boundary layer to progress from turbulent, to transitional, to laminar; this condition results in a large increase in extent of separation). More recently, this trend in extent of laminar and transitional separations with Reynolds number has been discussed in reference 23.

The present data show a trend in the extent of separation with Reynolds number that is characteristic of laminar boundary layers. This effect can be seen for nonablating models by comparing figures 10(a) and 10(b) for the cylinder-flare model, and figures 11(a) and 11(b) for the base model (differences in the amount of boundary-layer cooling between the two test conditions are negligible). The pressure distributions at the higher Reynolds numbers (figs. 10(a) and 11(a)) are characteristic of separated flows; those at the lower Reynolds numbers (figs. 10(b) and 11(b)) are characteristic of attached flows. Separation and reattachment, or the absence of separation, shown schematically in figures 10 and 11, were determined as described earlier.

In line with the previous discussion, the behavior of the separated regions reported in reference 21 appears to be typically transitional. Gray (ref. 21), in fact, recognized that transition was at or near reattachment in his experiments. Such a location of transition is certainly supported by the fact that the length Reynolds numbers were very high; also shadowgraphs of the separated flows in reference 21 are typical of those shown in reference 22 for transitional boundary layers. However, Gray ignored the importance of transition to the extent of separation in redefining a laminar separation to include the case where transition was at or near reattachment. The data in reference 21 should have been compared with other data for transitional separations.

Influence of Reynolds Number on the Surface Pressures for the Nonablating Hemisphere-Cylinder Model

The ratio of surface pressure to pitot pressure for the nonablating hemispherical-nosed model without a flare decreased as the Reynolds number was decreased (cf. figs. 10(a) and 10(b)). Possible orifice effects caused by the low pressure and high temperature do not account for this trend. This result was not expected because the opposite trend has generally been observed. In reference 24, for example, a decrease in Reynolds number caused an increase in surface pressure. This was attributed to a change in the effective body shape resulting from a change in displacement-thickness growth close to the nose. The significant difference between the present experiments and those discussed in reference 24 is believed to be that the Reynolds number in the present experiments was so low that the viscous layer was beginning to merge with the shock wave. Reference 25 suggests that large reductions in surface

pressures that have been observed on flat plates as Reynolds number was reduced might be due to the merging of viscous layer and shock wave. It is possible that the present experiments are in the regime where the influence of a merged viscous layer and shock wave predominates over the influence of a displacement thickness growth.

Effects of Ablation on Extent of Separation and on Surface Pressures

The effects of ablation on the extent of separated regions and on the pressure distributions are shown in figures 12 to 17 for the three model shapes. Many flow-visualization photographs were used to determine the extent of separated flow; a few representative photographs are shown (figs. 13(d), 13(e), and 15(b)). Variations in the extent of separated flows can be determined approximately from changes that occur in the pressure distributions. The pressure distributions shown are for all the combinations of models and test conditions that were investigated. At the low Reynolds number condition, the pressures on ablating models were time dependent; the pressures shown in figures 15 to 17 were measured late in the run.

Nose ablation.- The extent of laminar separation, whether large or small, was not measurably affected by nose ablation. Furthermore, nose ablation did not cause separation where there was no separation on the nonablating models ($\theta = 25^\circ$ at the higher Reynolds number; $\theta \leq 45^\circ$ at the lower Reynolds number). The flow-visualization data in figure 13(d), for example, show by the size of the separation wedge that nose ablation had negligible influence on the extent of separation at the high Reynolds number. At the low Reynolds number, flow-visualization data indicated completely attached flow for both the nonablating and the ablating models; thus no influence of ablation on separation could be detected. The pressure distributions in figures 12 to 17 also indicate that ablation had little or no effect on the extent of separation (cf. figs. 10(a) and 10(b), and 11(a) and 11(b) for the distinguishing features in a pressure distribution that mark the presence of separation).

Nose ablation had little or no effect on surface pressures at the high Reynolds number, provided the boundary layer remained laminar (figs. 12-14), but at the low Reynolds number the pressures increased significantly for some of the ablation materials (figs. 15-17). The absence of any influence at the high Reynolds number could possibly be due to very low rates of gas injection -- the values of mass loss were moderate, but a large portion of this was liquid.

It is apparent from the data at the low Reynolds number that the magnitude of pressure increase depends on the ratio $\dot{m}/\dot{m}_\infty$ as well as on the particular material used (this is consistent with the conclusions of ref. 26). A discussion of the quantitative effect of injecting various gases into the boundary layer should, of course, include all properties of the ablation materials such as the ratio of melt to gas, and molecular weight of the injected gas, in addition to the value $\dot{m}/\dot{m}_\infty$ presently used. Such an analysis is beyond the scope of the present investigation.

Since nose ablation increased surface pressures well ahead of the flare on the hemispherical-nosed model, it is clear that this influence was caused by an alteration to the attached boundary layer that was in no way associated with separation or the adverse pressure gradient at the flare. The injection into the boundary layer of ablation gases that have zero streamwise velocity probably causes an increase in displacement thickness by flattening the velocity profile. (Calculated results in reference 26 show that injection did increase displacement thickness.) Such an increase in displacement thickness would be expected to increase surface pressures if other factors remained constant. The influence of mass injection by nose ablation shown by the present experiments is, in fact, very similar to the displacement-thickness effect discussed in the previous section. Reference 24 showed that this effect was largest near the nose (a case similar to that in fig. 15(a)) and increased as Reynolds number was decreased (a trend similar to that shown by comparing figs. 13(c) and 15(a)). It is important to note here that, as discussed above, the boundary layer and shock wave merged at the low Reynolds number for the hemispherical-nosed model. The change in displacement thickness due to ablation probably predominated over any increased merging of boundary layer and shock wave due to ablation because the largest changes to a boundary layer due to ablation would be expected to occur close to the surface, not at the edge of the boundary layer. It is believed, therefore, that the increased surface pressure near the compression corners for all the present model shapes is a result of displacement-thickness growth caused by ablation.

Flare ablation.- Flow-visualization data showed that flare ablation caused a very small increase in the extent of laminar separation. This is shown at the higher Reynolds number by the size of separation wedges and the location of oil accumulations in figure 13(e). At the lower Reynolds number a separated region appeared (shown by the unburned region on the ablating flare, fig. 15(b)) where there was formerly none (shown by the oil flowing up the flare, fig. 15(b)). The oil accumulation on the model with the ablating flare that is shown in figure 15(b) was about 0.1d upstream of the corner.

Flare ablation caused the cylinder pressures to increase. At the higher Reynolds number (fig. 13(c)), the pressure increase was probably due, in part, to the upstream movement of the separation point; an additional effect, indicated by the higher peak pressure, could result from boundary-layer thickening or a larger turning angle at separation. These effects of flare ablation were possibly caused by the gases from the ablating flare that were turned back into the large separated region. At the lower Reynolds number, the increased pressures (fig. 15(a)) apparently were a result of the appearance of a separated region, and an increased thickness of the flare shock layer due to ablation (this is faintly visible in the original photographs of fig. 15(b)).

Effect of Ablation on Boundary-Layer Transition

Data for the conical-nosed model indicated that ablation might have caused boundary-layer transition to occur on the model at the higher Reynolds number since unsteady flow near separation was indicated by fluctuating pressures. Reference 22 showed that separated flows were unsteady when transition was at the separation point, whereas separated flows were steady for all other locations of transition. The pressure data for the model with the 35° flare are shown in figure 18(a). The pressures were steady only on the model with the smooth, nonablating nose; the separated region shown is for the steady flow. The pressure data for the ablating noses, shown by the symbols, represent average values indicated by the transducers. The pressure-measuring system could not respond accurately to fluctuating pressures; however, these data are useful as an indicator that unsteady flow did occur. The odd shape of some of the distributions is characteristic of that measured with a system with long tubing when the flow is unsteady (see fig. 19 in ref. 22). The pressures on the model with the 25° flare were steady because no separation occurred (see fig. 14). The pressures near separation for the 45° flare were steadier than for the 35° flare. Apparently the 45° flare caused separation sufficiently far ahead of transition that the unsteadiness was reduced (see fig. 18(b)).

Transition on the ablating models could have been affected by both surface roughness of the ablating material and by the injection of ablation gases into the boundary layer. The relative importance of each is not known. To learn whether gas injection contributed to early transition, the importance of roughness will be examined. As a basis for comparison, roughness was added to the nonablating cone as shown in the lower right photograph of figure 19. The roughness consisted of 5 rings with square edges about $0.04d$ high, spaced at approximately even increments along the cone, beginning at about $0.4d$ from the tip (the ratio of roughness height to δ^* was probably much greater for this nose than for any of the ablating noses, especially for the first 3 rings). This roughness caused transition near the separation point as evidenced by very unsteady pressures. The Teflon nose (upper, left photograph in fig. 19) was always smooth, but surface pressures in the separated region were slightly unsteady, indicating that transition could have been at the separation point a small portion of the time. (Since this model remained smooth, ablation must have been the important factor.) The unsteadiness was the least (judging from the amplitude of pressure fluctuations) that was observed for the three ablating materials, but so was the ablation rate. For this case, the breakdown to turbulent flow was probably just beginning near the separation point, whereas it likely was further advanced for the other models. The surface roughness of the phenolic nylon nose varied considerably during the run, as shown by the three lower photographs on the left side of figure 19. The phenolic nylon was initially smooth. Early in the run a wave of melt flowed back over the nose (two middle photographs on the left). Later, the surface was fairly smooth, except for the accumulation of melt near the cone-cylinder juncture (lower, left). The postrun condition of the phenolic nylon nose is shown in the upper right photograph of figure 19. Although the accumulation of melt increased the diameter of the model near the base of the cone, the protuberances were primarily smooth blisters in the shape of spherical segments with a small height-to-chord ratio. Furthermore,

the ratio of roughness height to displacement thickness was generally small near the cone-cylinder juncture. This roughness was probably not very important to transition; however, unsteadiness of surface pressures in the separated region indicated that transition was again at the separation point.

It appears that the roughness on the nonablating cone was much more severe than that on any of the ablating cones, but that the location of transition was about the same for all these noses. If the slight roughness on the ablating cones had been primarily responsible for the occurrence of transition at separation, then the severe roughness would likely have caused transition upstream of separation (the resulting turbulent boundary layer would have been easily detectable). Since this did not occur, it is concluded that the roughness on the ablating models was not solely responsible for causing transition at the separation point because it is not probable that this small roughness, in itself, could cause transition at the same location as for the severe roughness on the nonablating cone. It is believed, therefore, that gas injection by ablation played a significant part in causing early transition on the ablating models. (This is consistent with the result in ref. 27 that illustrates that suction delays transition, and with ref. 28 that shows that blowing causes early transition.) Quantitatively, the small ablation rates associated with these conical noses (1 to 2 percent of $\dot{m}_\infty$) seem to be as important to transition as the severe roughness on the nonablating nose. (Delrin was excluded from this discussion because its high ablation rate relative to Teflon and phenolic nylon is misleading due to the large amount of melt.) An approximate transition Reynolds number based on free-stream properties and the model length to the cylinder-flare juncture was about 61,000. The significance of this number is not known, however, because the Reynolds number for natural transition is not known for the present test facility.

Nose ablation could cause large changes in the extent of separation if ablation caused transition to move from downstream of reattachment to upstream of separation. The possible change in the extent of separation would be the largest at high Reynolds numbers where laminar separations are large (ref. 1), and where transition on the nonablating model is near reattachment. The resulting turbulent boundary layer would, under most circumstances, be attached (see ref. 20).

Time Dependent Pressures

Surface pressures were time dependent at the low Reynolds number test condition only. An example is shown in figure 20. In the early portion of the run, slow time response of the pressure system was a major factor in the pressure increase with time. Later in the run, when the rate of pressure rise was much less, the pressure system was probably able to respond to the pressure changes. The time dependency of pressures shown in the latter portion of the run therefore likely represents actual pressure changes on the model with time. Although the pressure level was time dependent, no change in the extent of separation with time was observed.

The increase in surface pressure with time is believed to have been due to variations of model temperature and of the ablation rate. The change in model temperature (about 110° K in a typical test with a nonablating model) probably caused the displacement thickness to increase slightly, resulting in a slight increase in surface pressure. This increase is apparent for the nonablating model in figure 20. The most notable change in the ablating model during a run was the blunting of the nose as a result of ablation. The shape of the nose had no direct effect on the surface pressures, however, as shown by the data in figure 20 for the nonablating model that had a nose shape equivalent to the final shape of the Delrin nose. Instead, the blunting of the ablating nose is believed to have increased the rate of ablation ($\dot{m}/m_\infty$), thus causing a time dependent increase of the displacement thickness.

Effect of Cylinder Diameter on Separation for the Base Model

Base-flow models were tested with two sizes of cylinders in order to estimate the influence of cylinder diameter on the base-flow separation. Data for the models with a cylinder diameter of 3.81 cm have been presented in previous sections; the extent of separation was well defined by both oil flow and pressure distributions. Extent of separation on the models with a cylinder diameter of 1.27 cm was detected by oil flow only. The oil accumulations on the 45° base models (fig. 21(a)) indicate that the location of separation at high Reynolds number was not significantly affected by the 3 to 1 change in cylinder diameter. The shape of the separated regions for these two models is compared in figure 21(b) by superimposing the models, and the locations of the oil accumulations at separation and the limits for which both upstream and downstream oil flow was observed at reattachment. If reattachment was at the midpoint of the regions bounded by the upstream and downstream oil flow, it appears from figure 21(b) that the size of the cylinder had little or no influence on the shape of the separated base flow. A similar situation occurred for the 35° base; for this model, however, the extent of separation was less than for the 45° base (cf. figs. 12(b) and 12(c), for example).

Effect of Nose Shape on the Extent of Laminar Separation

The separated region on the cylinder-flare model with the conical nose was larger than on the cylinder-flare model with the hemispherical nose (cf. figs. 13(b) with 18(a) and 13(c) with 18(b)). Nose blunting decreases local Mach number and Reynolds number; thus two opposing effects result -- the reduced Mach number tends to increase the extent of separation and the reduced Reynolds number tends to decrease separation (see ref. 1). The resultant influence on the extent of separation depends upon which variable predominates (e.g., ref. 20 shows that for turbulent boundary layers one variable might predominate for some conditions, whereas, the other will predominate for other conditions -- probably the laminar boundary layer behaves in a similar manner). Previous investigations (refs. 1 and 20) have also shown that the extent of separation varied with nose shape, but that the conditions for incipient separation (and therefore the size of separation) were not affected by nose shape, provided values of local flow Mach number and Reynolds number

were used in the data correlations. Data at the present test conditions are insufficient for determining whether these data also correlate on the basis of local flow conditions.

Incipient Separation

Flare and base angles for incipient, laminar separation were determined only approximately because large angle increments were used. At the high Reynolds number, incipient separation on nonablating models occurred between 25° and 35° for each configuration; this range can, however, be narrowed down by considering the extent of flow separation on the models with the 35° flare or base. A very small separation occurred on the hemispherical-nosed model (figs. 6(d) and 13(b)), whereas larger separations occurred on the conical-nosed model (fig. 18(a)) and on the base-flow model (figs. 6(h) and 12(b)). The angle for incipient separation was, therefore, close to 35° for the hemispherical-nosed model and probably closer to 25° for the other two models. At the low Reynolds number, the angle for incipient separation was greater than 45° for all models. These large turning angles with no separation are consistent with results obtained at low Reynolds numbers that are presented in reference 2.

The conditions for incipient separation on the ablating models were very close to the incipient separation conditions for the nonablating models. This is implied by the present data that showed that ablation did not significantly alter the extent of laminar separation.

CONCLUDING REMARKS

Separated and attached flows have been studied on ablating and on nonablating models at a Mach number of 13.8. The boundary layers on these highly cooled models were generally laminar, but in a few cases appeared to have been transitional. The viscous layers were very thick -- at some conditions the boundary layer merged with the shock wave. A probable result of this merging of shock wave and boundary layer is the decrease in surface pressures that was observed for the attached flows as Reynolds number was decreased.

The laminar boundary layers in the present investigation turned very large expansion and compression angles with no separation. As Reynolds number was decreased, separation disappeared for even the 45° compression corner. For this case the boundary layer (and the layer that contained the ablation gases) nearly filled the shock layer. On the base model, a flow expansion from the stagnation point of 135°, followed by a recompression of 45°, occurred with no separation.

Nose ablation had no influence on the extent of laminar separation; however, flare ablation caused a small increase in the extent of separation, or caused a small separated region to appear where there was formerly none. This implies that ablation has little or no influence on incipient separation.

Ablation caused cylinder pressures to increase significantly in some cases, indicating that the boundary layers were altered by ablation even though the extent of separation was not largely affected. Apparently this influence was in no way associated with separation, as is indicated by the effect of nose ablation on the pressures well ahead of the separated regions. Instead, the pressure rise is believed to have been due to growth of the boundary-layer displacement thickness caused by ablation. With flare ablation, at the lower Reynolds number, an additional increase in pressure was associated with the appearance of separation and a thickened flare-shock layer.

Ablation appeared to have reduced the transition Reynolds number. At high Reynolds numbers where laminar separations are generally large and where transition is near reattachment, ablation could, therefore, cause very large decreases in the extent of separation if it causes the boundary layer to change from laminar to turbulent.

Ames Research Center
National Aeronautics and Space Administration
Moffett Field, Calif., 94035, March 21, 1967
129-01-09-02-00-21

REFERENCES

1. Kuehn, Donald M.: Laminar Boundary-Layer Separation Induced by Flares on Cylinders at Zero Angle of Attack. NASA TR R-146, 1962.

2. Kuehn, Donald M.: Laminar Boundary-Layer Separation Induced by Flares on Cylinders With Highly Cooled Boundary Layers at a Mach Number of 15. NASA TN D-2610, 1965.

3. Kuehn, Donald M.; and Monson, Daryl J.: Boundary-Layer Separation and Reattachment With and Without Ablation. Presented at the AGARD Specialist's Meeting on Separated Flows (Rhode-Saint-Genese, Belgium), May 10-13, 1966.

4. Eschenbach, R. C.; and Skinner, G. M.: Development of Stable, High Power, High Pressure Arc Air Heaters for a Hypersonic Wind Tunnel. WADD TR 61-100, July 1961.

5. Fay, J. A.; and Riddell, F. R.: Theory of Stagnation Point Heat Transfer in Dissociated Air. J. Aero. Sci., vol. 25, no. 2, Feb. 1958, pp. 73-85, 121.

6. Hansen, C. Frederick: Approximations for the Thermodynamic and Transport Properties of High-Temperature Air. NACA TN 4150, 1958.

7. Inouye, Mamoru: Blunt Body Solutions for Spheres and Ellipsoids in Equilibrium Gas Mixtures. NASA TN D-2780, 1965.

8. Cheng, H. K.: Hypersonic Shock-Layer Theory of the Stagnation Region at Low Reynolds Number. Proc. Heat Transfer and Fluid Mechanics Institute, Stanford Univ. Press. 1961, pp. 161-175.

9. Jorgensen, Leland H.: The Total Enthalpy of a One-Dimensional Nozzle Flow With Various Gases. NASA TN D-2233, 1964.

10. Reinhardt, Walter A.; and Baldwin, Barrett S., Jr.: A Model for Chemically Reacting Nitrogen-Oxygen Mixtures With Application to Nonequilibrium Air Flow. NASA TN D-2971, 1965.

11. Wentink, Tunis W., Jr.: High Temperature Behavior of Teflon. AFBMD TN 59-15, July 1959.

12. Steg, L.; and Lew, H.: Hypersonic Ablation, The High Temperature Aspects of Hypersonic Flow. Proc. AGARD-NATO Specialist's Meeting (Rhode-Saint-Genese, Belgium), 1962, W. C. Nelson, ed., The Macmillan Co., 1964, pp. 629-680.

13. Kratsch, K. M.; Hearne, L. F.; and McChesney, H. R.: Thermal Performance of Heat Shield Composites During Planetary Entry. Paper presented at the AIAA-NASA National Meeting, Palo Alto, Calif., Sept. 30 to Oct. 1, 1963.

14. Lundell, John H.; Wakefield, Roy M.; and Jones, Jerold W.: Experimental Investigation of a Charring Ablative Material Exposed to Combined Convective and Radiative Heating. AIAA J., vol. 3, no. 11, Nov. 1965, pp. 2087-2095.

15. Garr, Leonard J.; and Marrone, Paul V.: Inviscid, Nonequilibrium Flow Behind Bow and Normal Shock Waves. Part II. The IBM 704 Computer Programs. CAL QM-1626-A-12(II), May 1963.

16. Probstein, Ronald F.; and Kemp, Nelson H.: Viscous Aerodynamic Characteristics in Hypersonic Rarefied Gas Flow. J. Aerospace Sci., vol. 27, no. 3, March 1960, pp. 174-192, 218.

17. Ivanov, A. V.: Density Near the Forward Critical Point of a Blunt Body in a Supersonic Rarefied Gas Flow. Soviet Physics - Doklady, vol. 10, no. 3, Sept. 1965, pp. 191-193.

18. Clutter, Darwin W.; and Smith, A. M. O.: Solution of the General Boundary-Layer Equations for Compressible Laminar Flow, Including Transverse Curvature. Rep. LB 31088, Douglas Aircraft Co., Feb. 15, 1963.

19. Inouye, Mamoru; and Lomax, Harvard: Comparison of Experimental and Numerical Results for the Flow of a Perfect Gas About Blunt-Nosed Bodies. NASA TN D-1426, 1962.

20. Kuehn, Donald M.: Turbulent Boundary-Layer Separation Induced by Flares on Cylinders at Zero Angle of Attack. NASA TR R-117, 1961.

21. Gray, J. Don: Laminar Boundary-Layer Separation on Flared Bodies at Supersonic and Hypersonic Speeds. AEDC-TDR 64-277, Jan. 1965.

22. Chapman, Dean R.; Kuehn, Donald M.; and Larson, Howard K.: Investigation of Separated Flows in Supersonic and Subsonic Streams With Emphasis on the Effect of Transition. NACA TR 1356, 1958.

23. Needham, David A.; and Stollery, John L.: Boundary Layer Separation in Hypersonic Flow. AIAA Paper 66-455, 1966.

24. Wagner, Richard D., Jr.; and Watson, Ralph: Reynolds Number Effects on the Induced Pressures of Cylindrical Bodies With Different Nose Shapes and Nose Drag Coefficients in Helium at a Mach Number of 24. NASA TR R-182, 1963.

25. McCroskey, W. J.; Bogdonoff, S. M.; and McDougall, J. G.: An Experimental Model for the Leading Edge of a Sharp Flat Plate in Rarefied Hypersonic Flow. AIAA Paper 66-31, 1966.

26. Thyson, N. A.; and Schurmann, E. E. H.: Blowing Effects on Pressure Interaction Associated With Cones. AIAA J. vol. 1, no. 9, Sept. 1963, pp. 2179-2180.

27. Schlichting, Hermann: Boundary-Layer Theory. Fourth ed., McGraw-Hill, Book Co., Inc., 1960.

28. Cresci, Robert J.; and Libby, Paul A.: The Downstream Influence of Mass Transfer at the Nose of a Slender Cone. J. Aerospace Sci., vol. 29, no. 7, July 1962, pp. 815-826.

TABLE I.- NOMINAL TEST CONDITIONS

Property	Condition 1 (high Reynolds number)	Condition 2 (low Reynolds number)
p_{t_1}, atm	67.0 ±2.0	10.0 ±0.3
$\dot{q}_{st}R_b^{1/2}$, J $m^{-3/2}$ sec^{-1}	(1.2 ±0.1)×10^5	(1.1 ±0.1)×10^5
h_{st}, J g^{-1}	(4.2 ±0.4)×10^3	(8.2 ±0.6)×10^3
p_{t_2}/p_{t_1}	(5.2 ±0.1)×10^{-4}	(7.6 ±0.3)×10^{-4}
M_∞	13.8	13.8
$Re_{\infty,d}$	9,000	1,000
$Re_{\infty,D}$	29,000	3,200
T_w/T_{st}	0.08 to 0.11	0.05 to 0.07

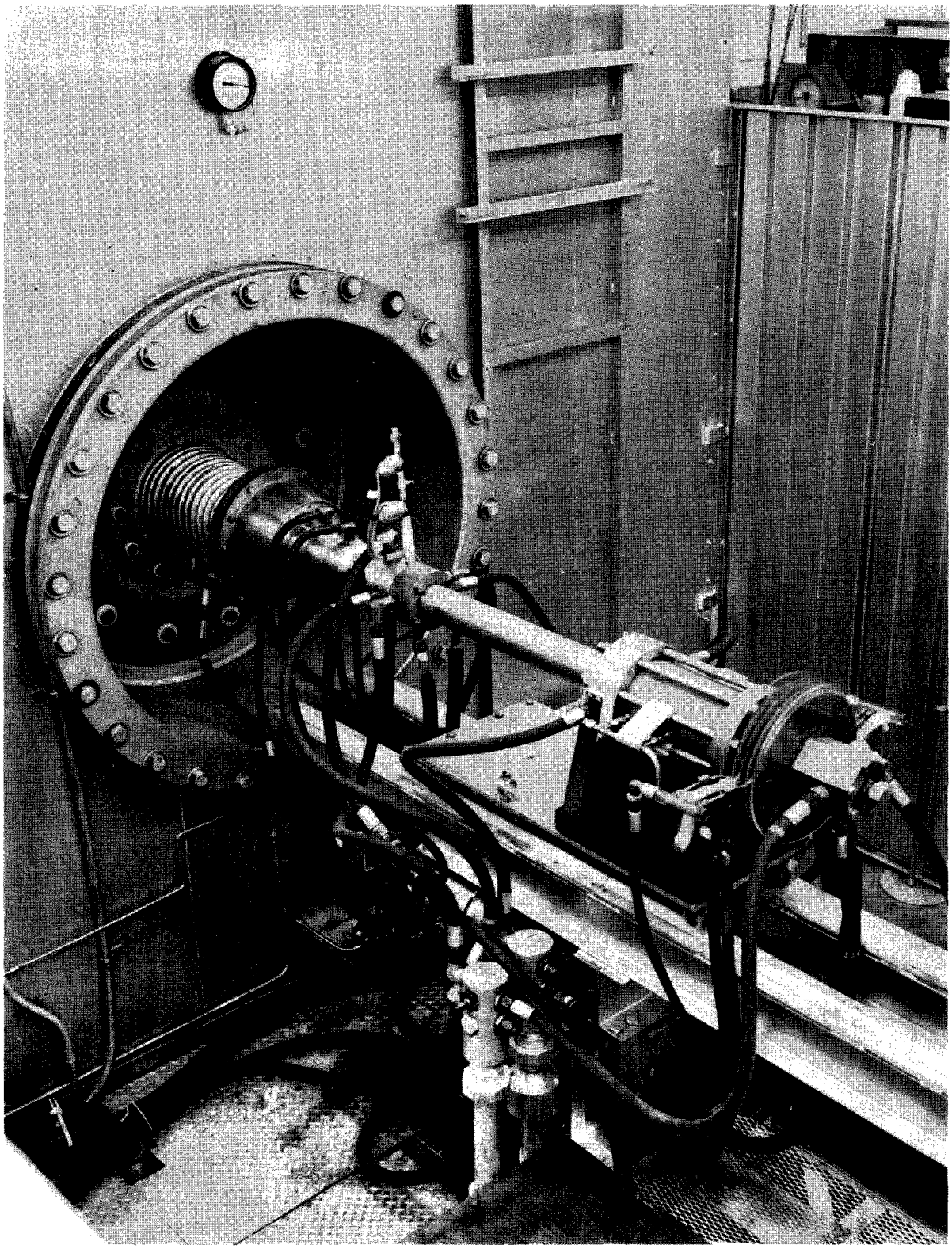

A-37814

Figure 1.- The Linde N-4000 arc heater.

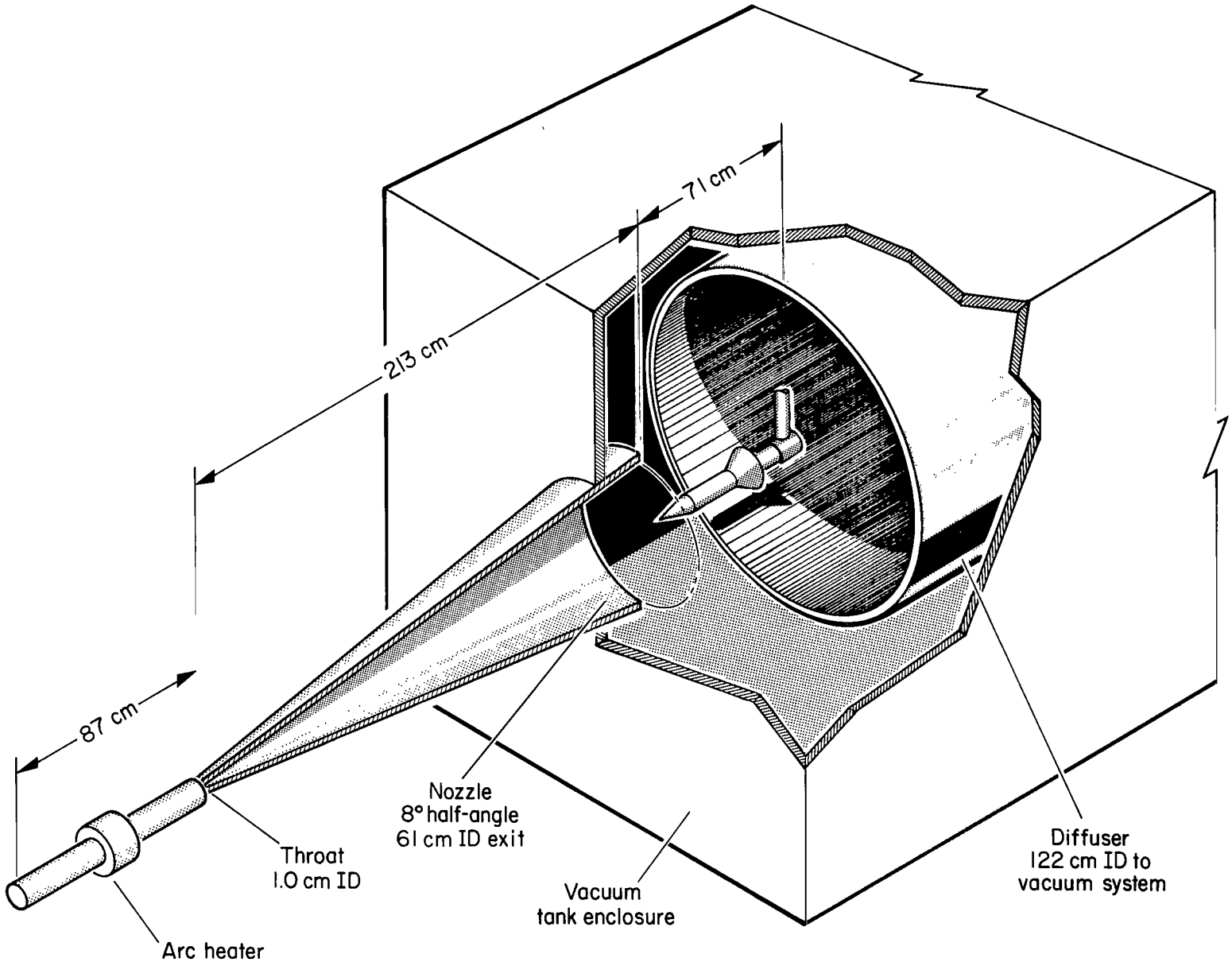

Figure 2.- Test facility.

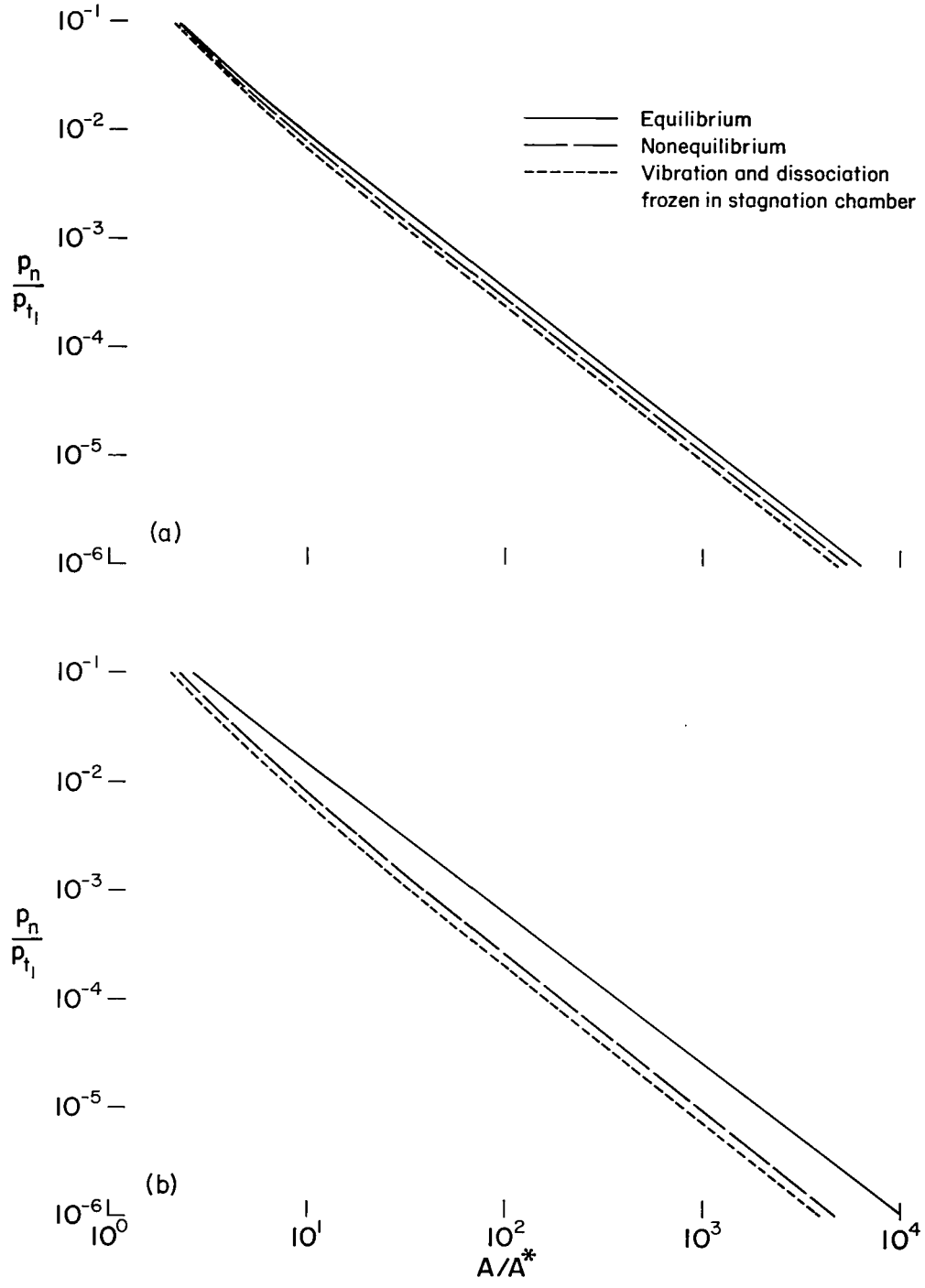

(a) High Reynolds number; p_{t_1} = 67 atm; h_{st} = 4.2×10^3 J/g.

(b) Low Reynolds number; p_{t_1} = 10 atm; h_{st} = 8.2×10^3 J/g.

Figure 3.- Variation of the theoretical static pressure along the nozzle center line.

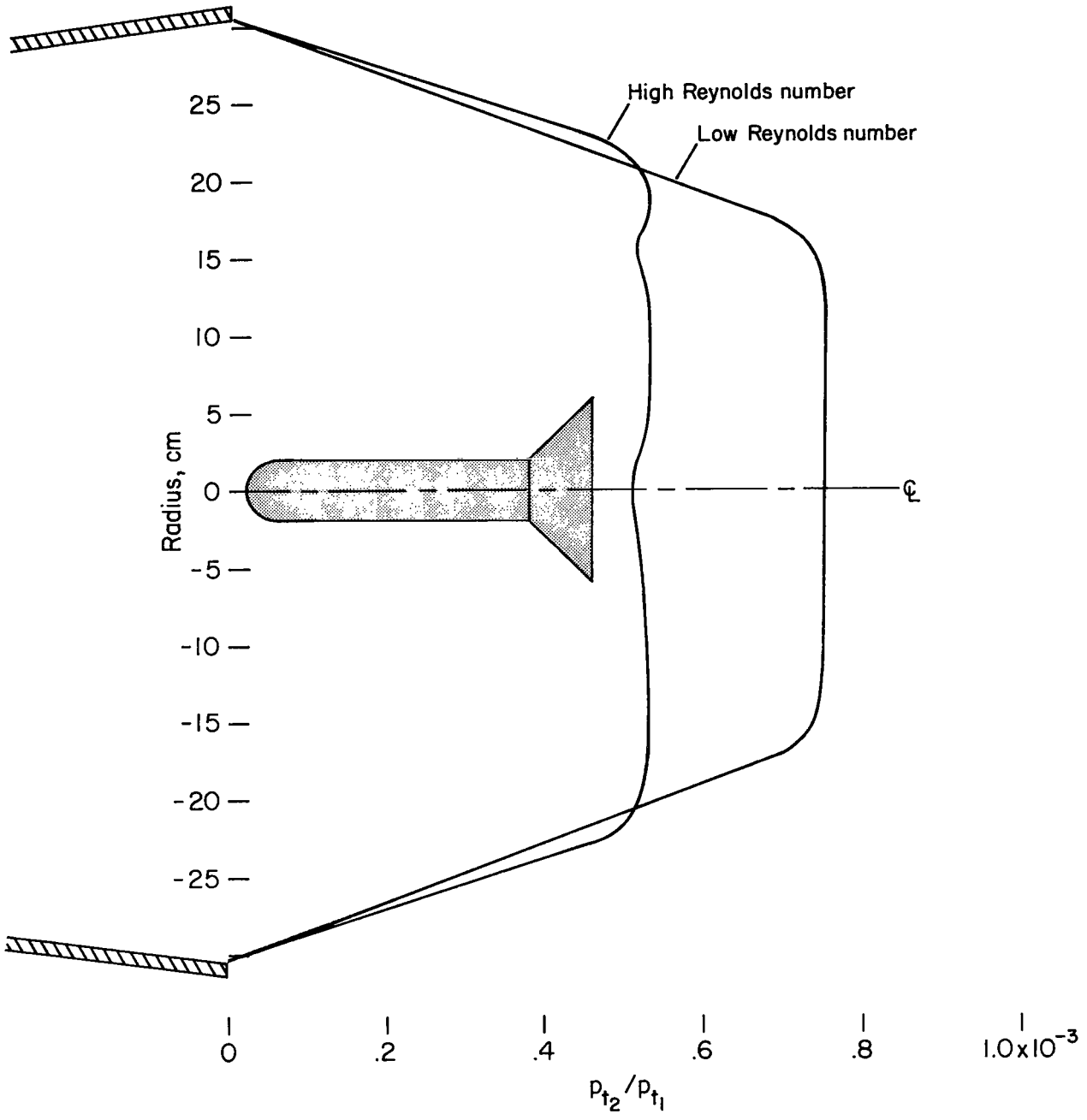

Figure 4.- Pitot pressure distribution in test stream.

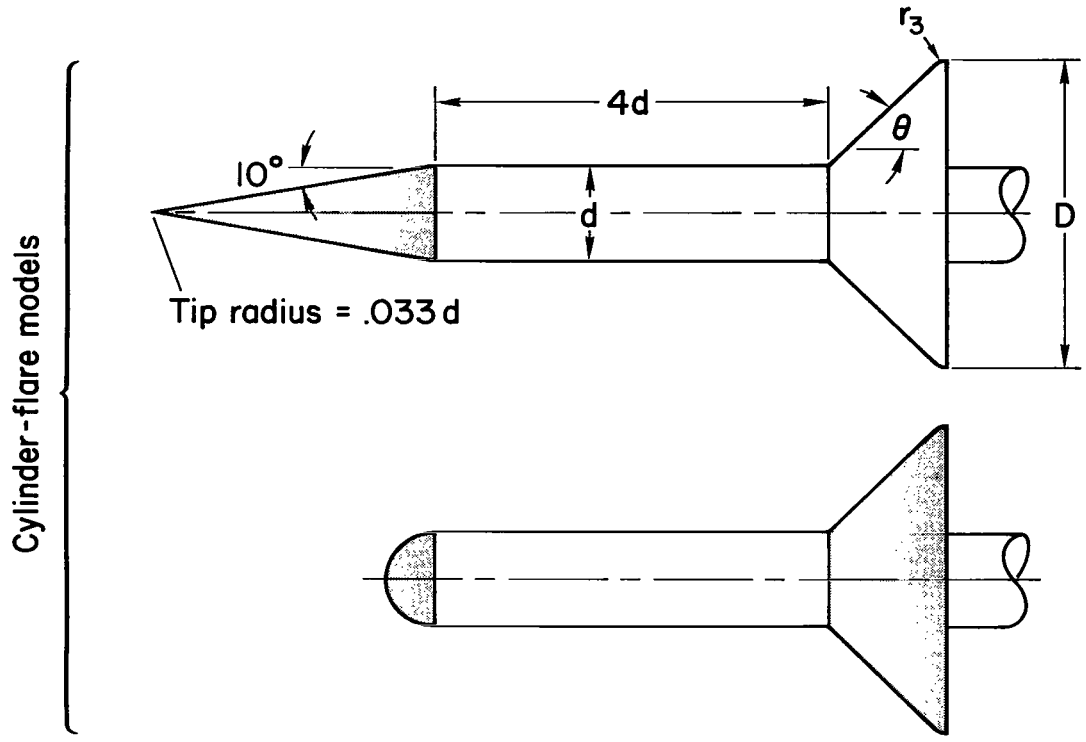

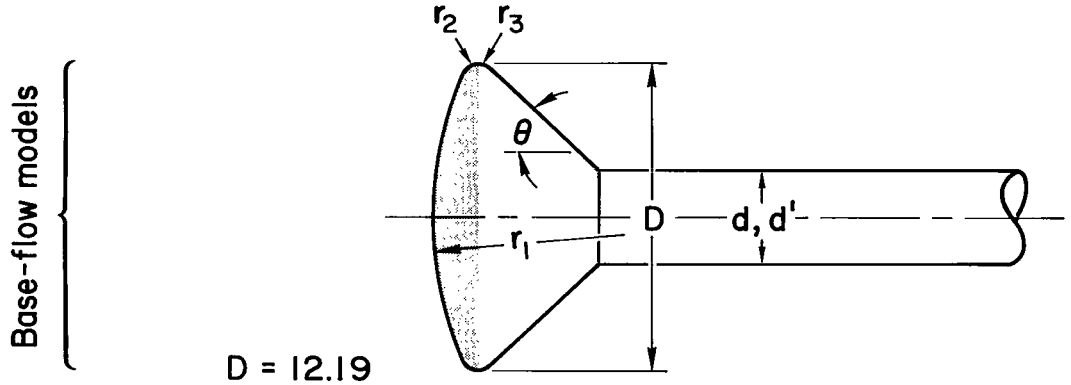

D = 12.19
d = 3.81
d' = 1.27
r_1 = 14.63
r_2 = 0.61

θ =	25°	35°	45°
r_3 =	2.46	1.15	0.61

Note: All dimensions in centimeters.
Shaded areas denote ablating surfaces.

Figure 5.- Models.

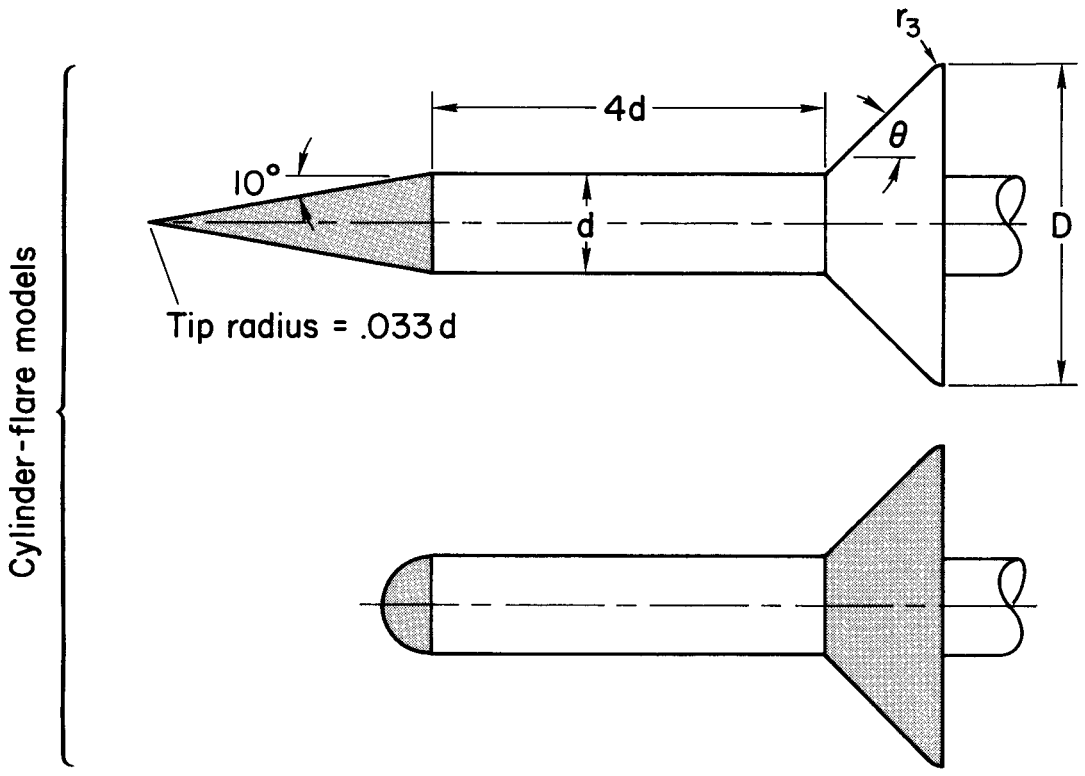

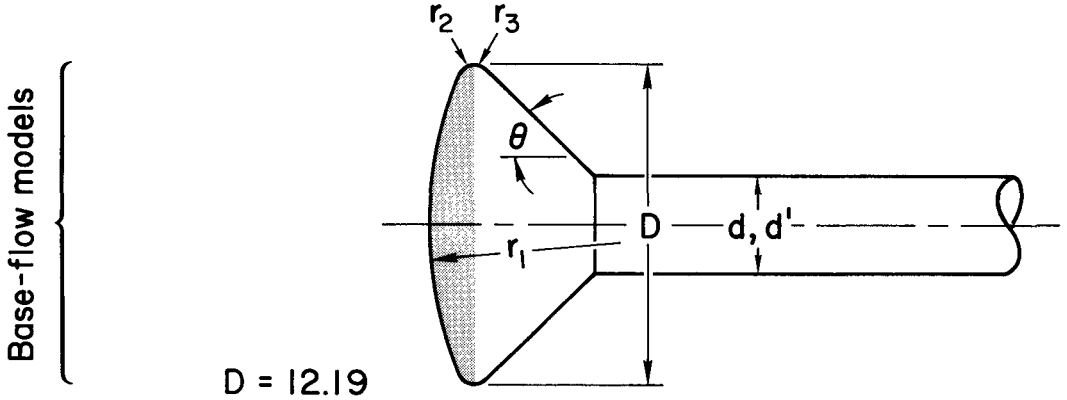

D = 12.19
d = 3.81
d' = 1.27
r_1 = 14.63
r_2 = 0.61

θ =	25°	35°	45°
r_3 =	2.46	1.15	0.61

Note: All dimensions in centimeters.
Shaded areas denote ablating surfaces.

Figure 5.- Models.

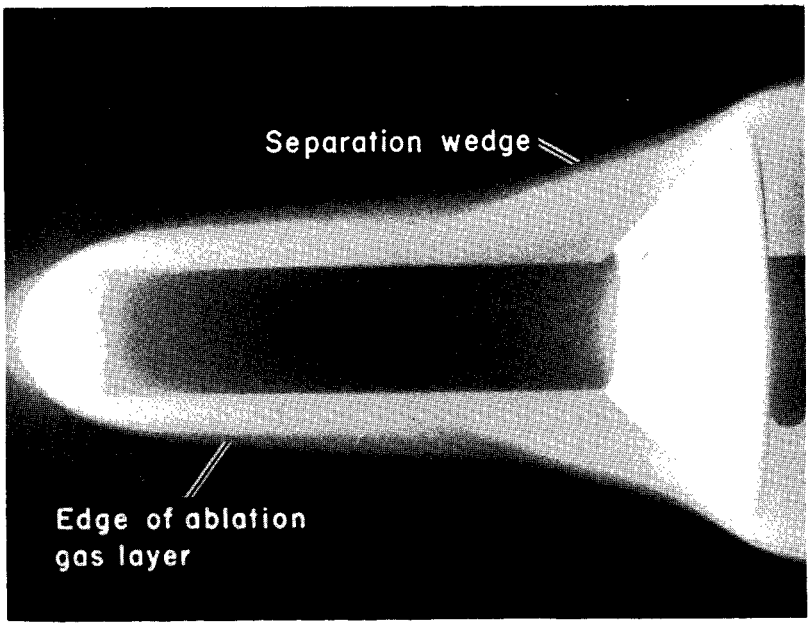

(a)

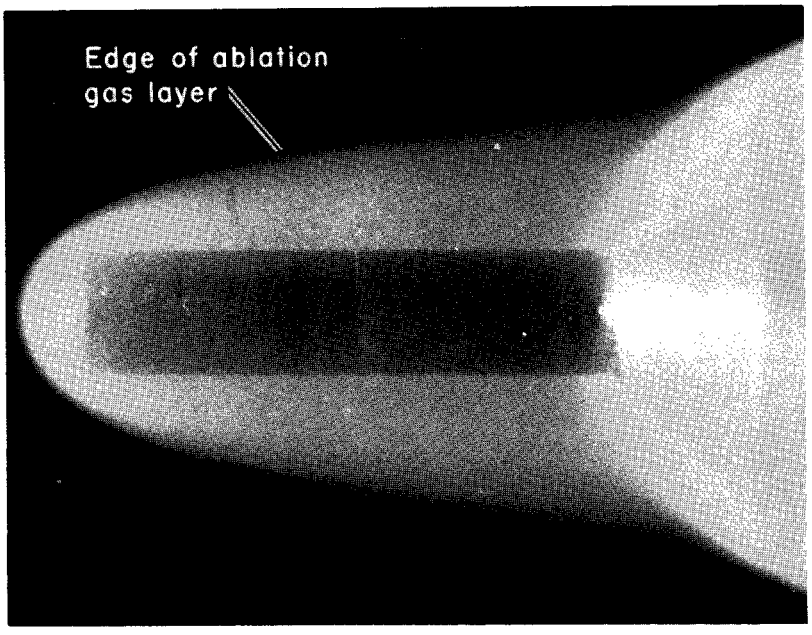

(b)

(a) Hemisphere-cylinder flare; phenolic nylon nose; $\theta = 45^{\circ}$; $Re_{\infty,d} = 9000$.
(b) Hemisphere-cylinder flare; phenolic nylon nose; $\theta = 45^{\circ}$; $Re_{\infty,d} = 1000$.

Figure 6.- Photographs that illustrate flow-visualization techniques.

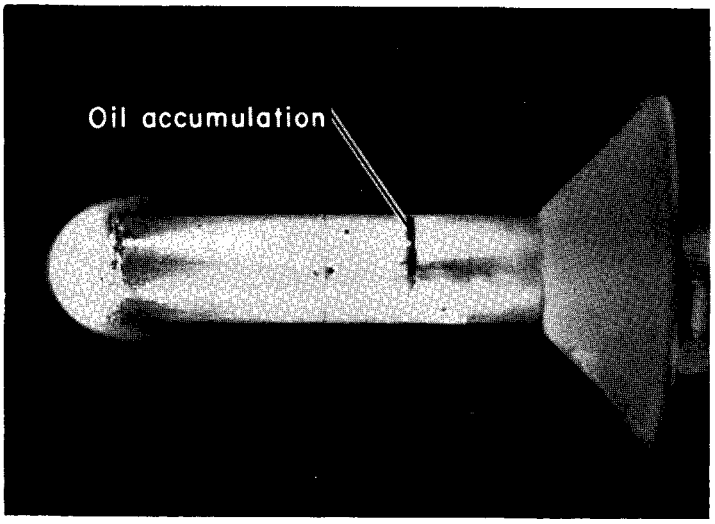

(c)

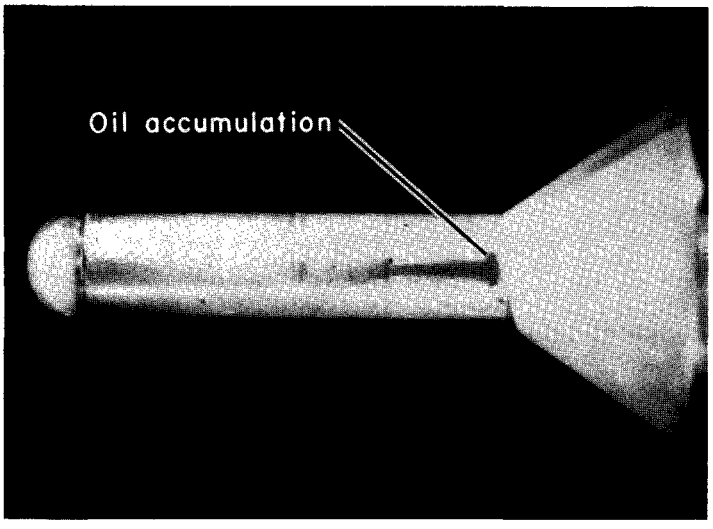

(d)

(c) Hemisphere-cylinder flare; phenolic nylon nose; $\theta = 45^{\circ}$; $Re_{\infty,d} = 9000$.
(d) Hemisphere-cylinder flare; nonablating nose; $\theta = 35^{\circ}$; $Re_{\infty,d} = 9000$.

Figure 6.- Continued.

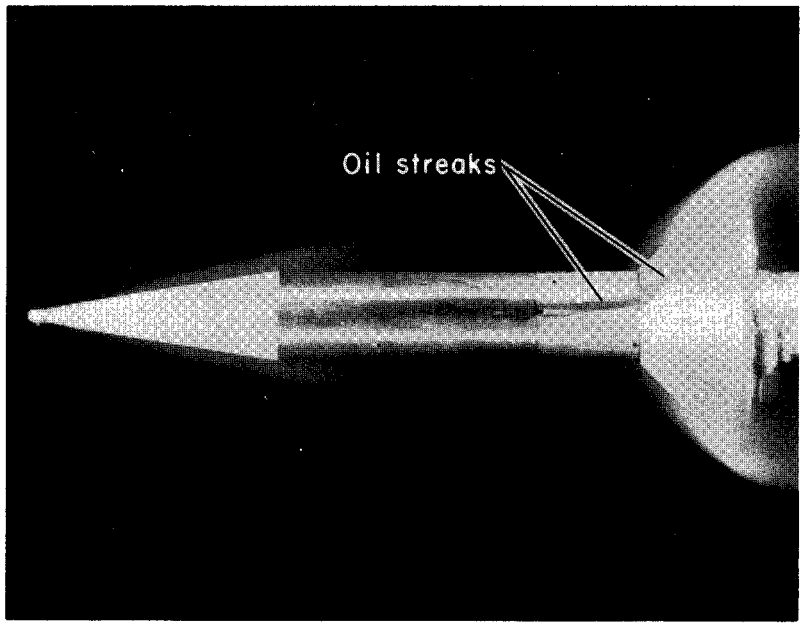

(e)

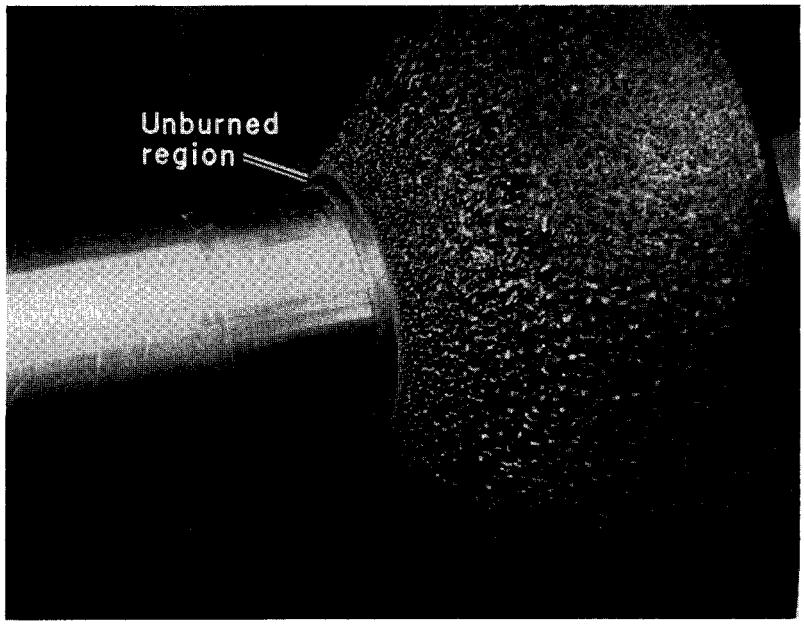

(f)

(e) Cone-cylinder flare; phenolic nylon nose; $\theta = 45^{\circ}$; $Re_{\infty,d} = 1000$.
(f) Post-run condition of phenolic nylon flare; phenolic nylon, hemispherical nose; $\theta = 45^{\circ}$; $Re_{\infty,d} = 1000$.

Figure 6. Continued.

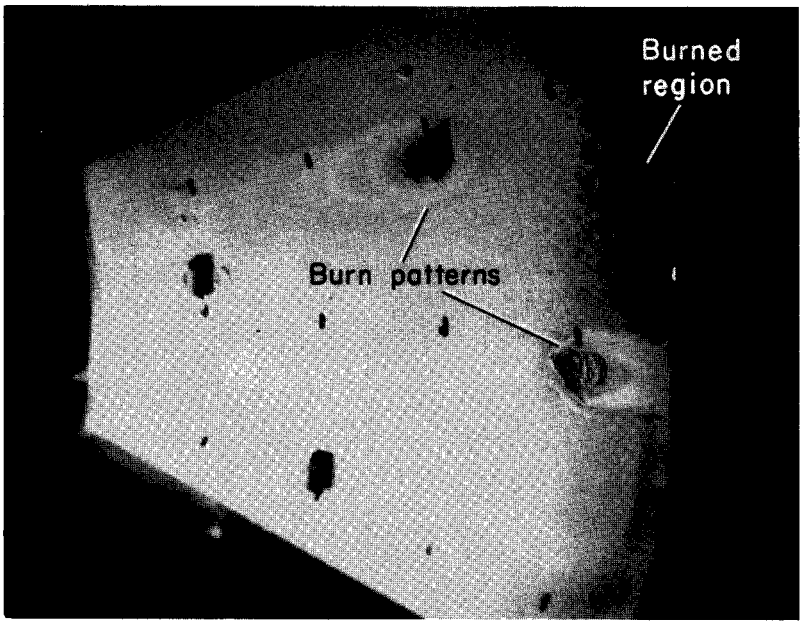

(g)

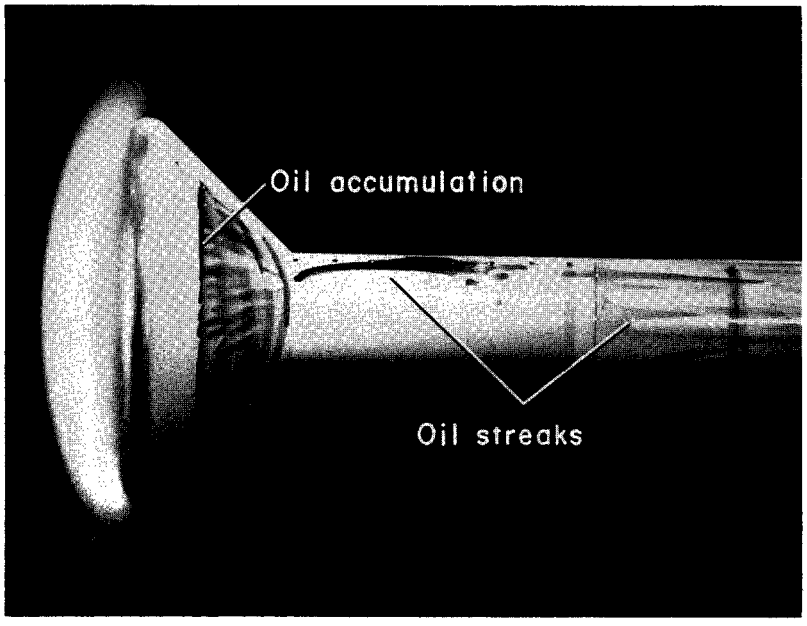

(h)

(g) Post-run condition of nonablating flare; nonablating, hemispherical nose; $\theta = 45^{\circ}$; $Re_{\infty,d} = 9{,}000$.
(h) Base-flow model; nonablating nose; $\theta = 45^{\circ}$; $Re_{\infty,D} = 29{,}000$.

Figure 6.- Continued.

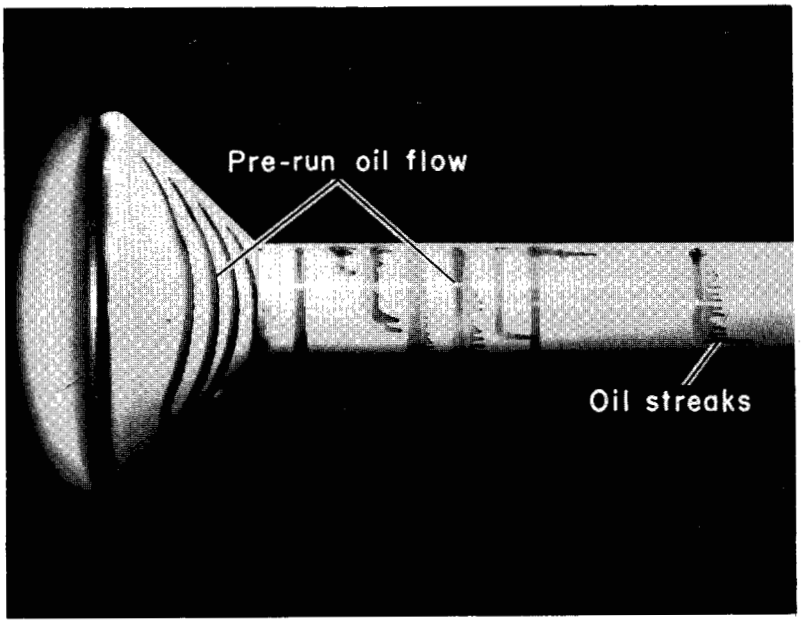

(i)

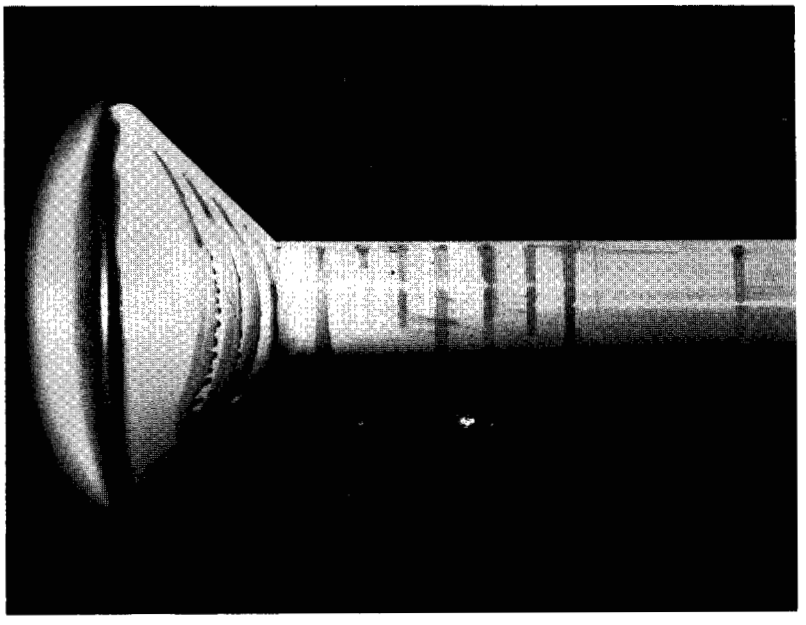

(j)

(i) Base-flow model; nonablating nose; $\theta = 45^{\circ}$; $Re_{\infty,D} = 3200$.
(j) Base-flow model; nonablating nose; $\theta = 45^{\circ}$; $Re_{\infty,D} = 3200$.

Figure 6.- Concluded.

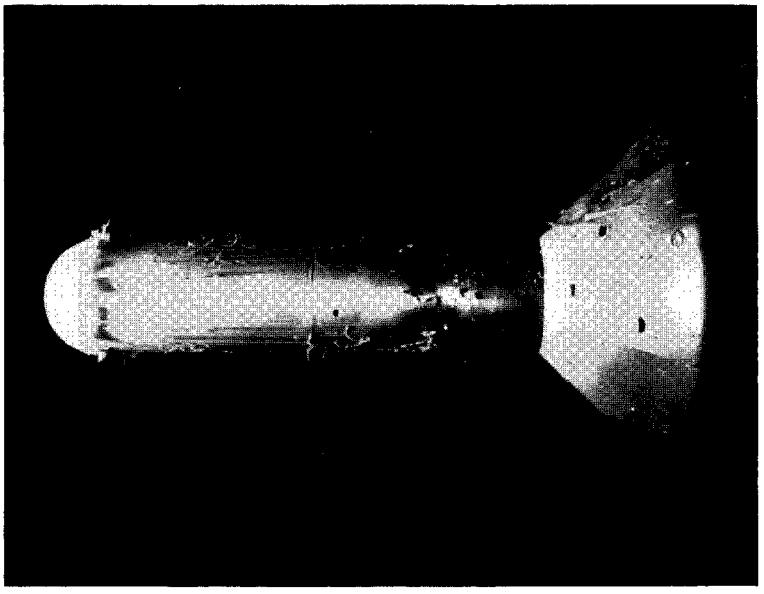

(a)

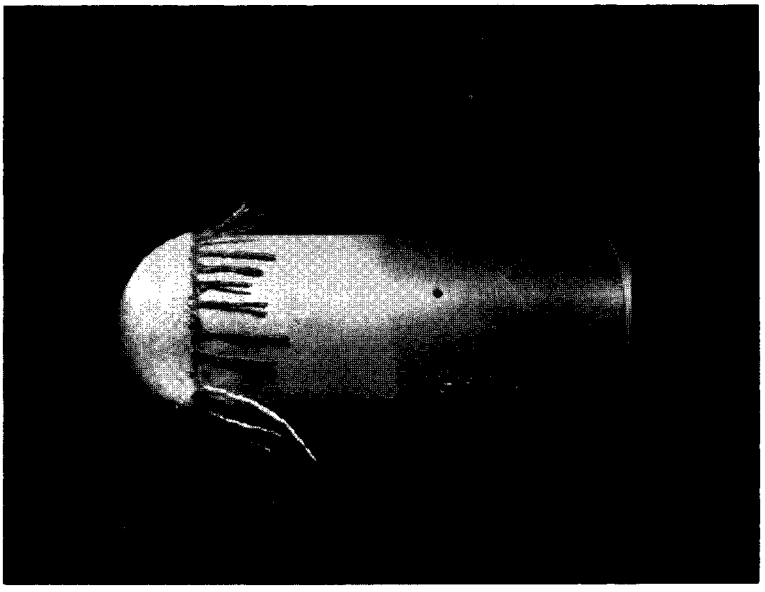

(b)

(a) $Re_{\infty,d}$ = 9000
(b) $Re_{\infty,d}$ = 1000

Figure 7.- Post-run photographs of the hemisphere-cylinder-flare models with Delrin noses.

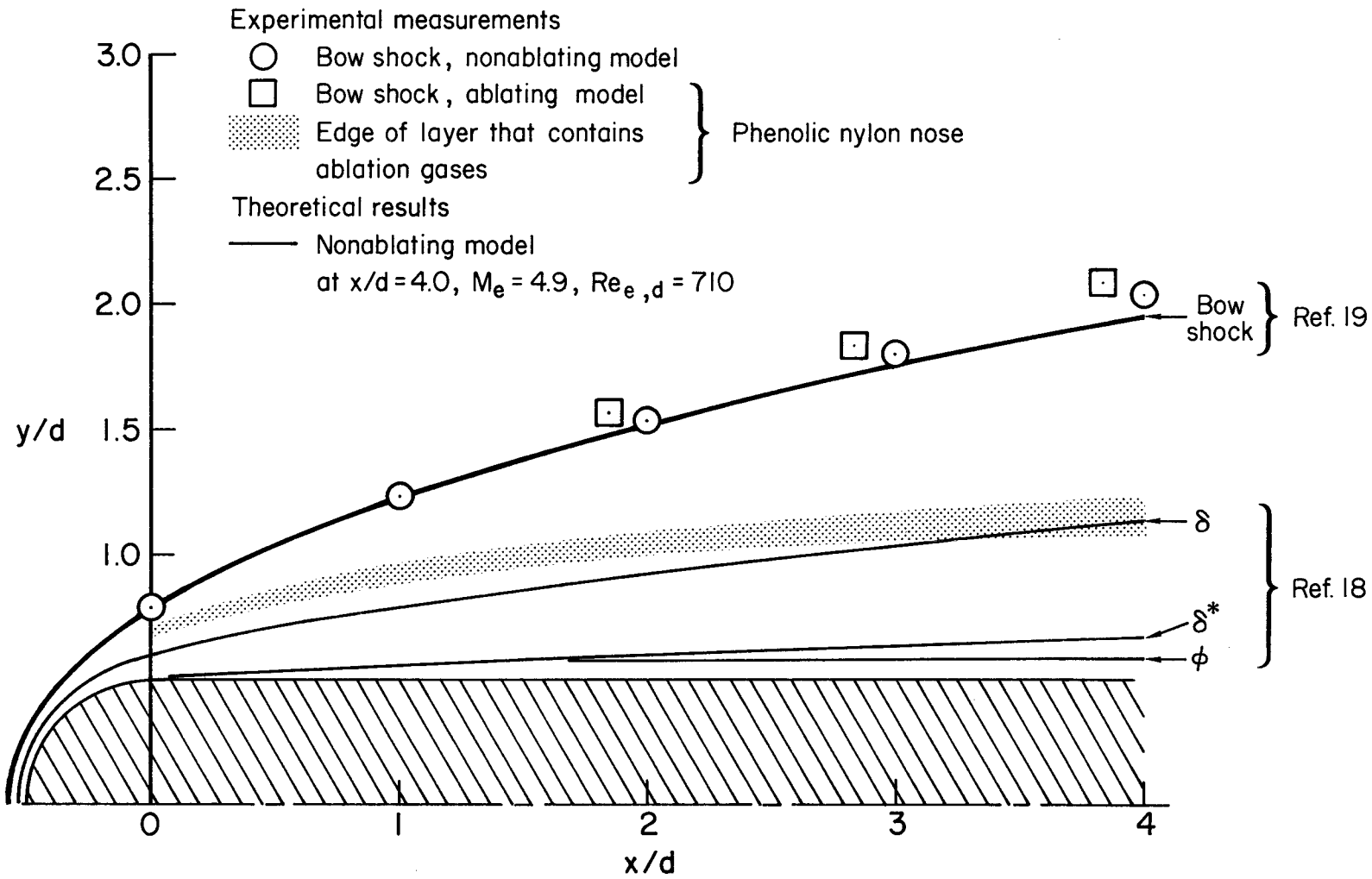

(a) $Re_{\infty,d}$ = 9000

Figure 8.- Boundary-layer velocity, displacement, and momentum thicknesses on the hemisphere-cylinder model.

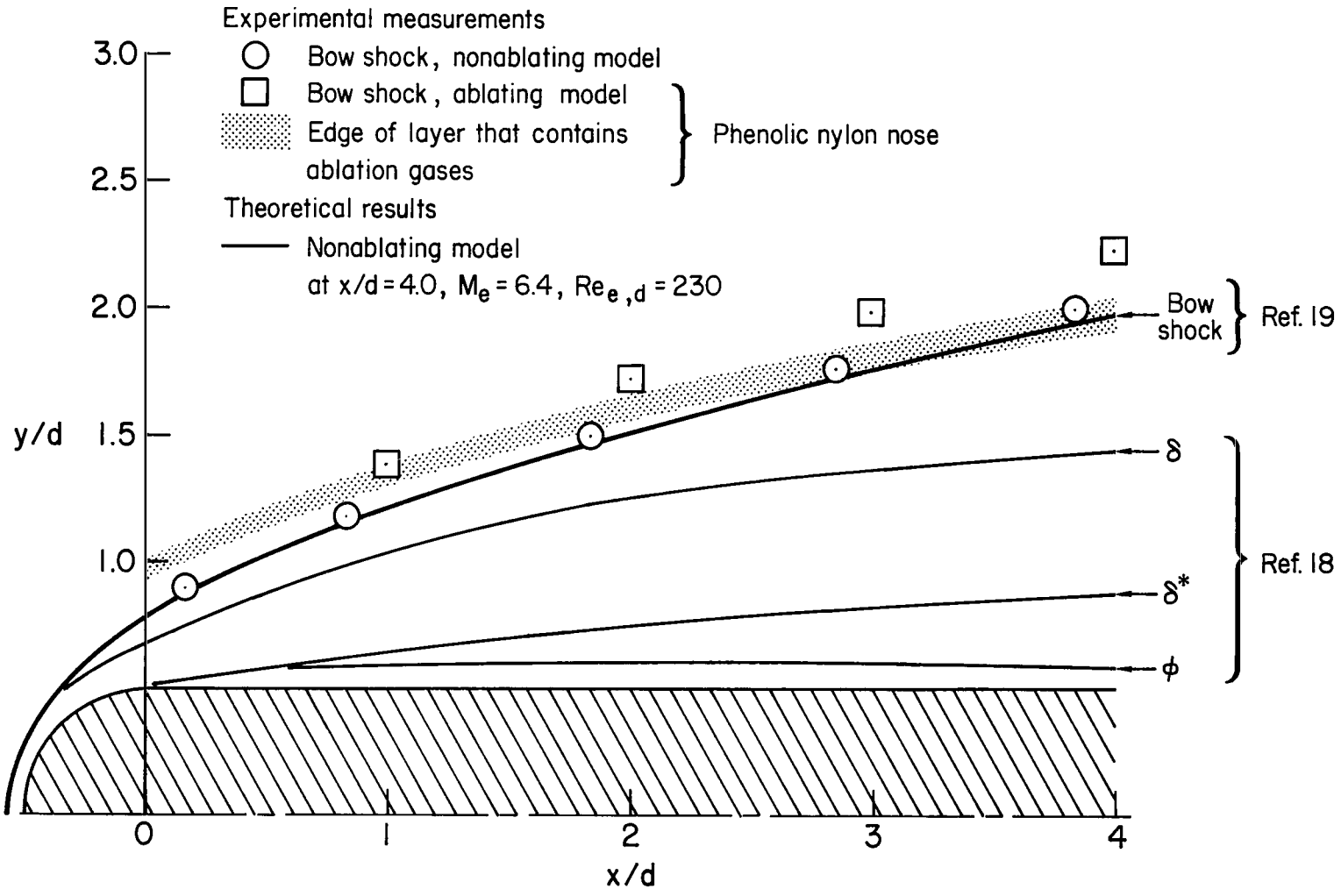

(b) $Re_{\infty,d}$ = 1000

Figure 8.- Concluded.

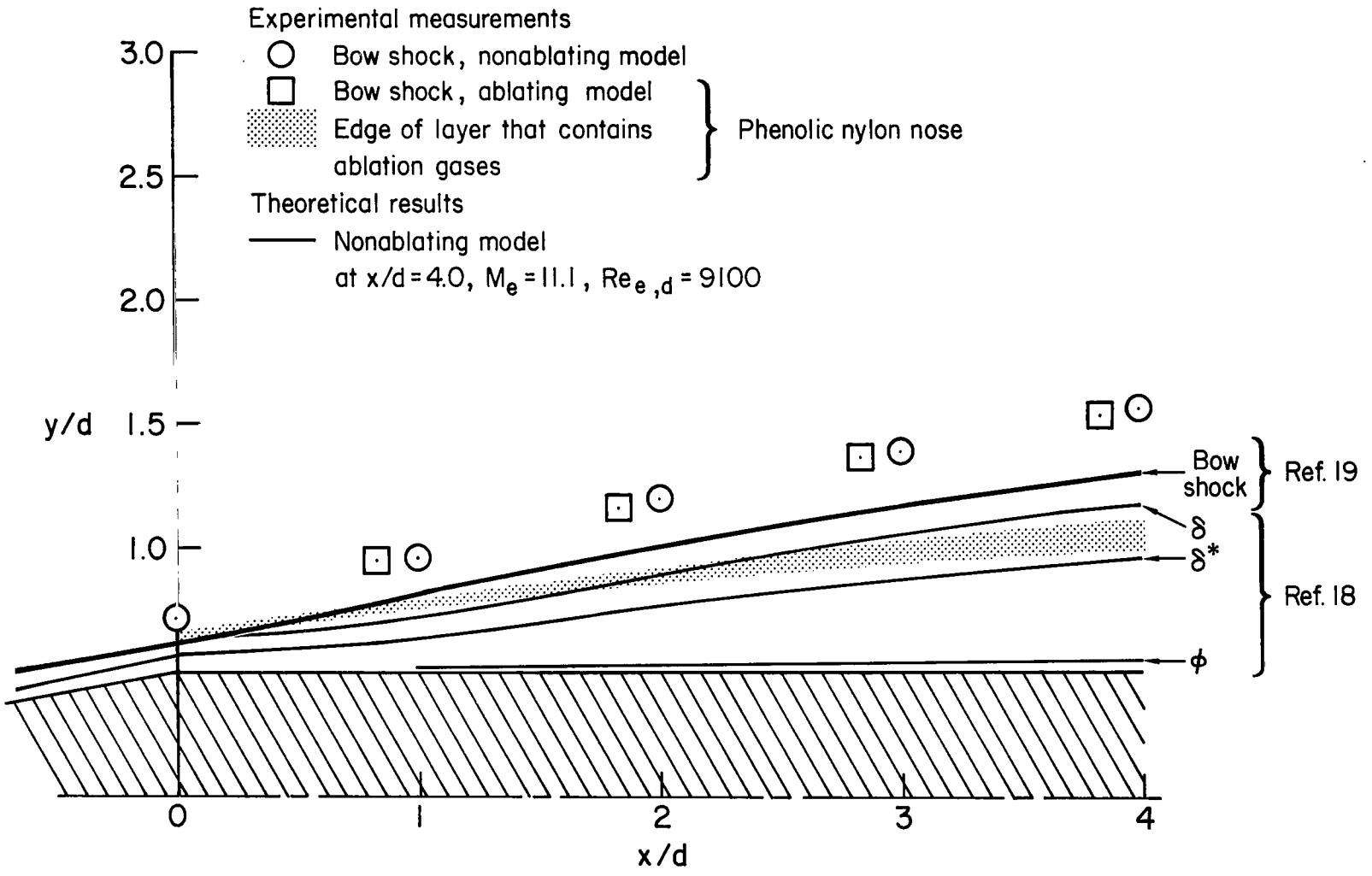

(a) $Re_{\infty,d}$ = 9000

Figure 9.- Boundary-layer velocity, displacement, and momentum thicknesses on the cone-cylinder model.

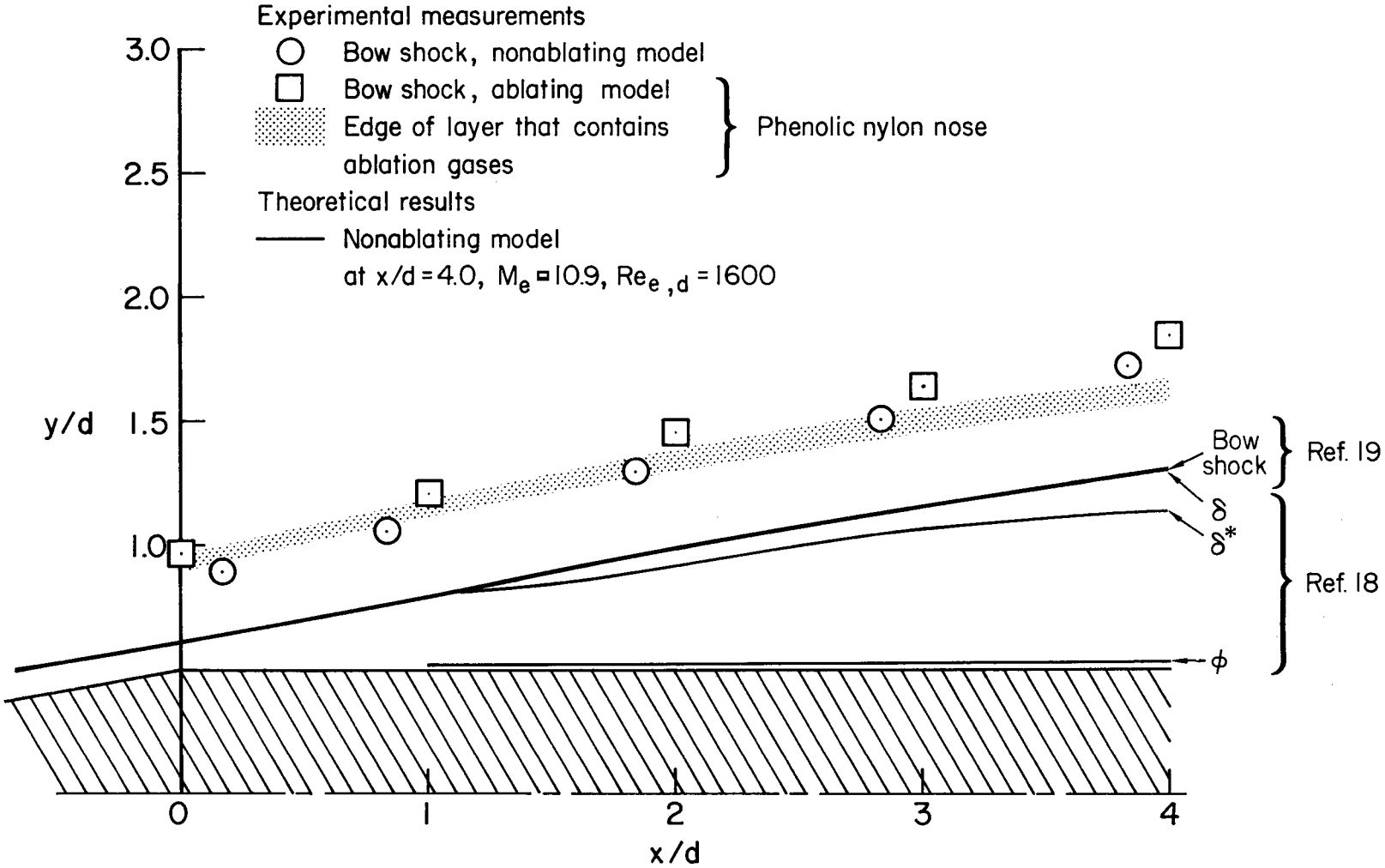

(b) $Re_{\infty,d}$ = 1000

Figure 9.- Concluded.

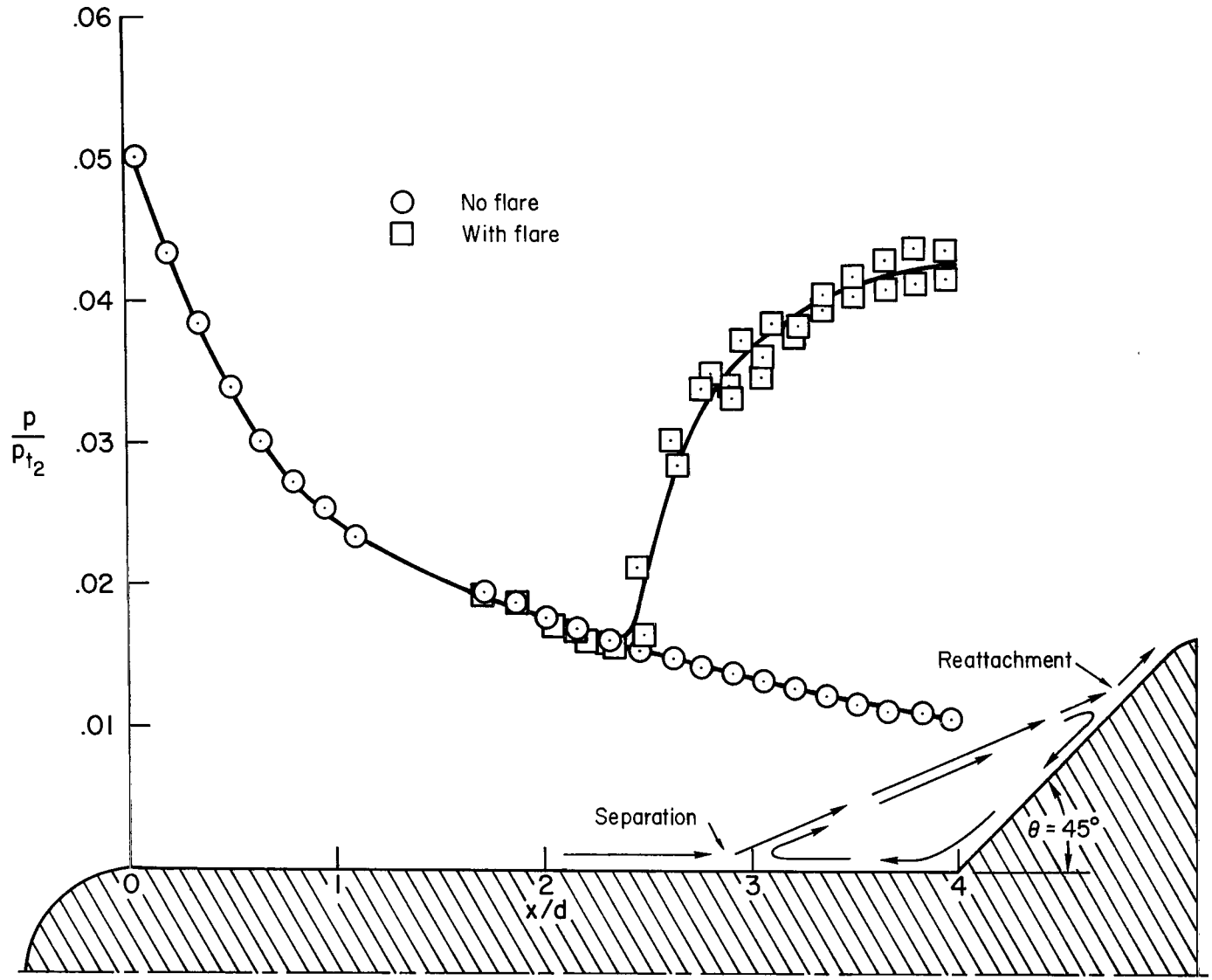

(a) $Re_{\infty,d}$ = 9000

Figure 10.- Effect of Reynolds number on the extent of laminar separation for the hemisphere-cylinder flare; θ = 45°; no ablation.

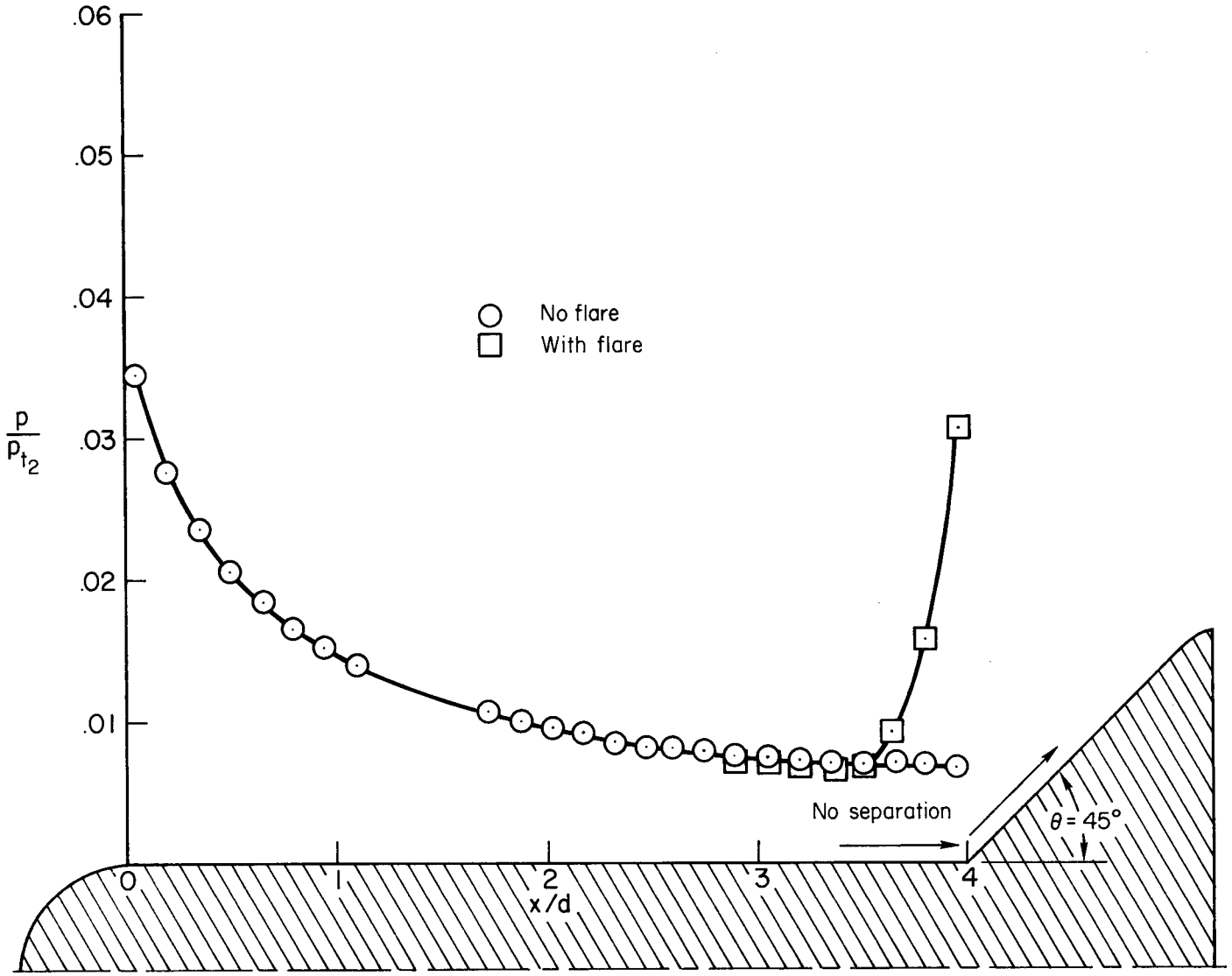

(b) $Re_{\infty,d} = 1000$

Figure 10.- Concluded.

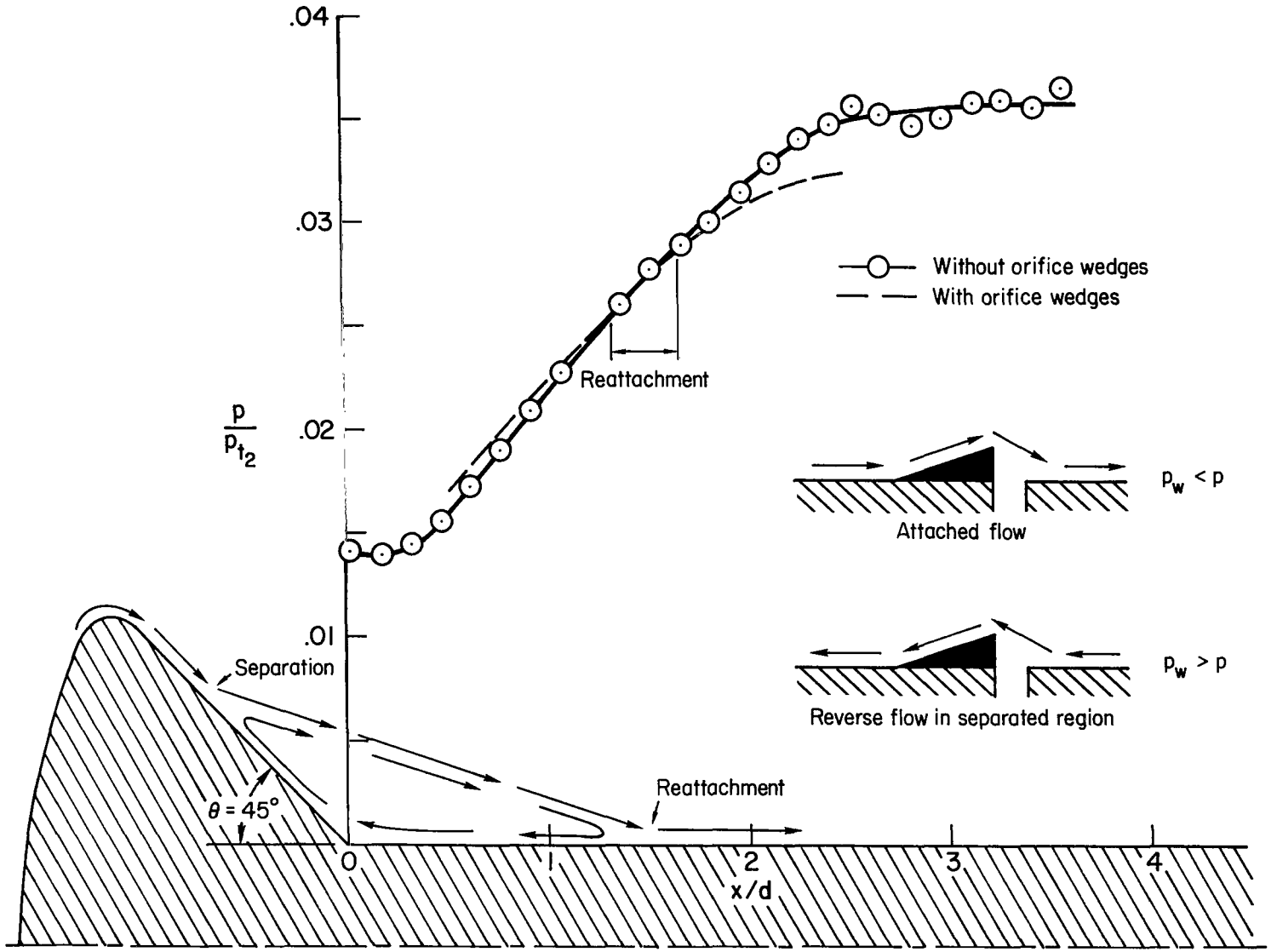

(a) $Re_{\infty,D}$ = 29,000

Figure 11.- Effect of Reynolds number on the extent of laminar separation for the base model; $\theta = 45^{\circ}$; no ablation.

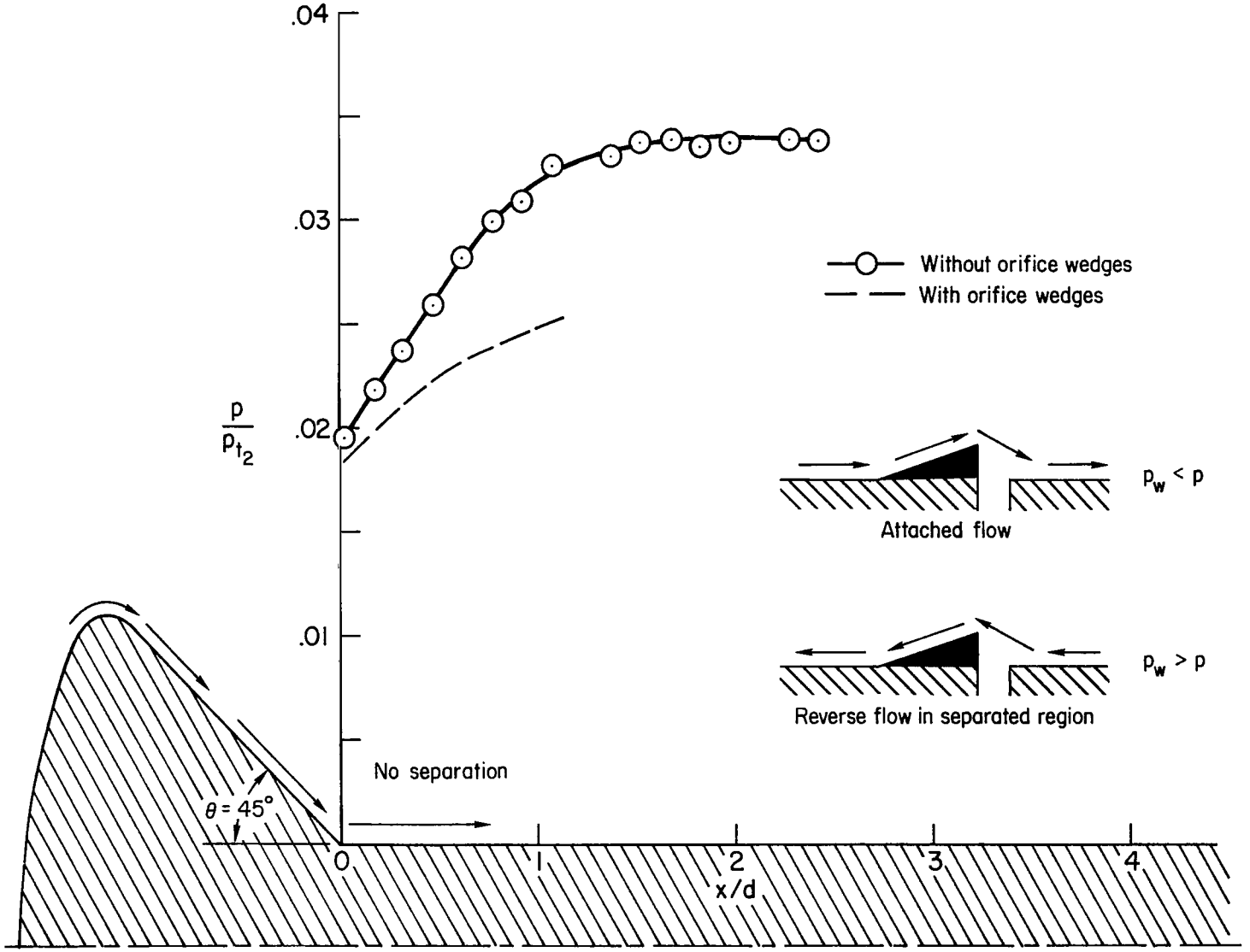

(b) $Re_{\infty,D}$ = 3200

Figure 11.- Concluded.

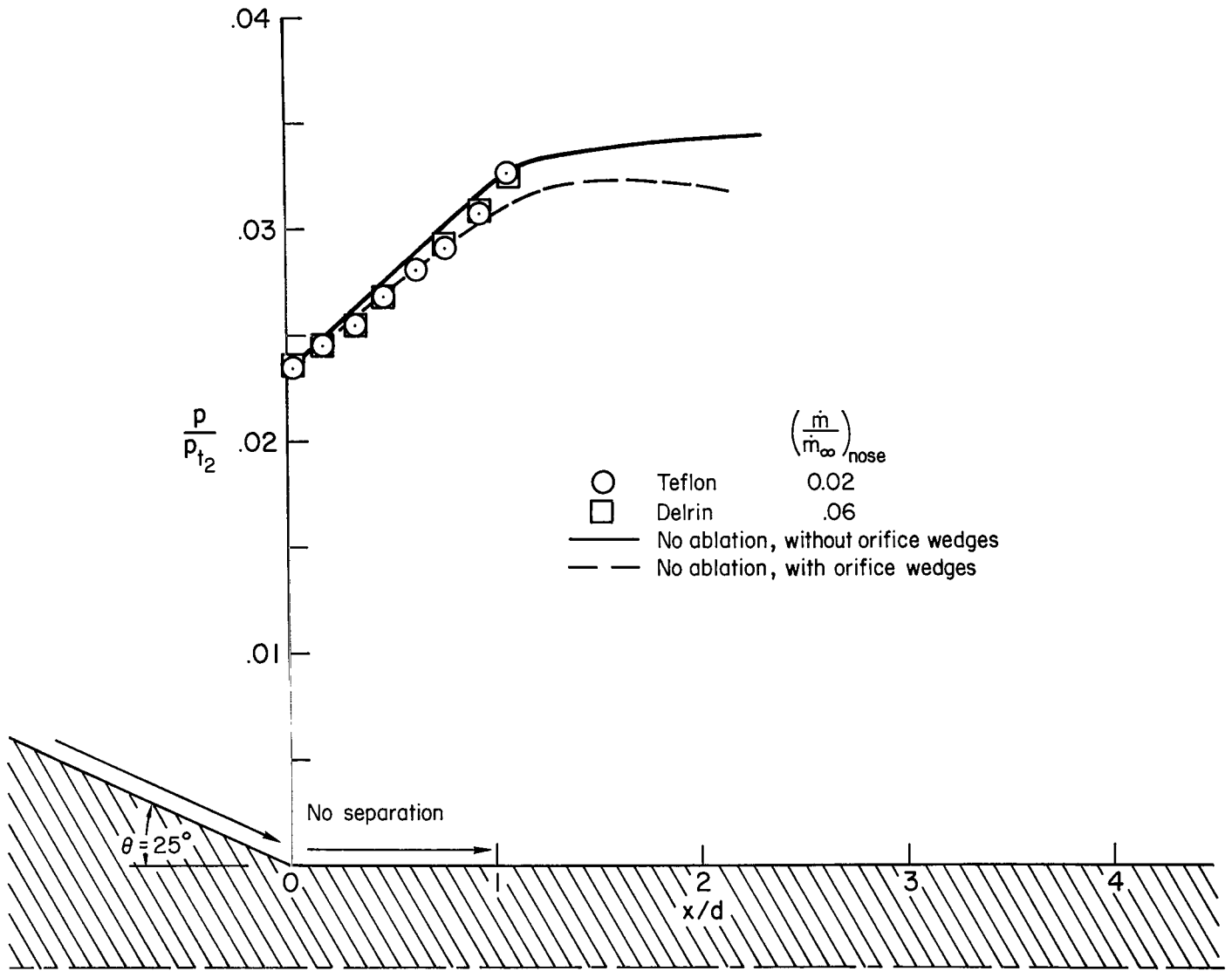

(a) $\theta = 25^{\circ}$

Figure 12.- Ablation effects for the base-flow model; $Re_{\infty,D} = 29,000$.

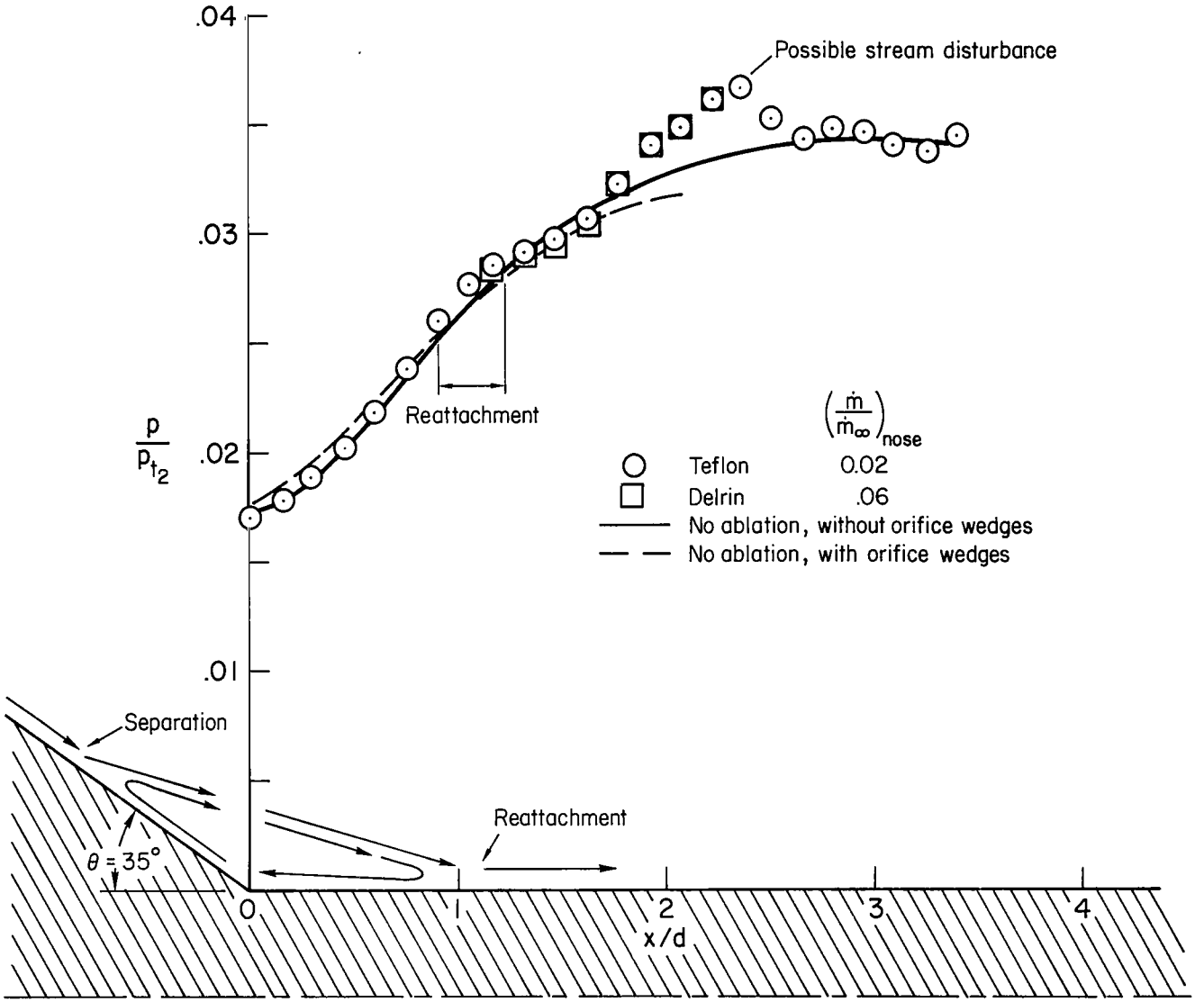

(b) $\theta = 35°$

Figure 12.- Continued.

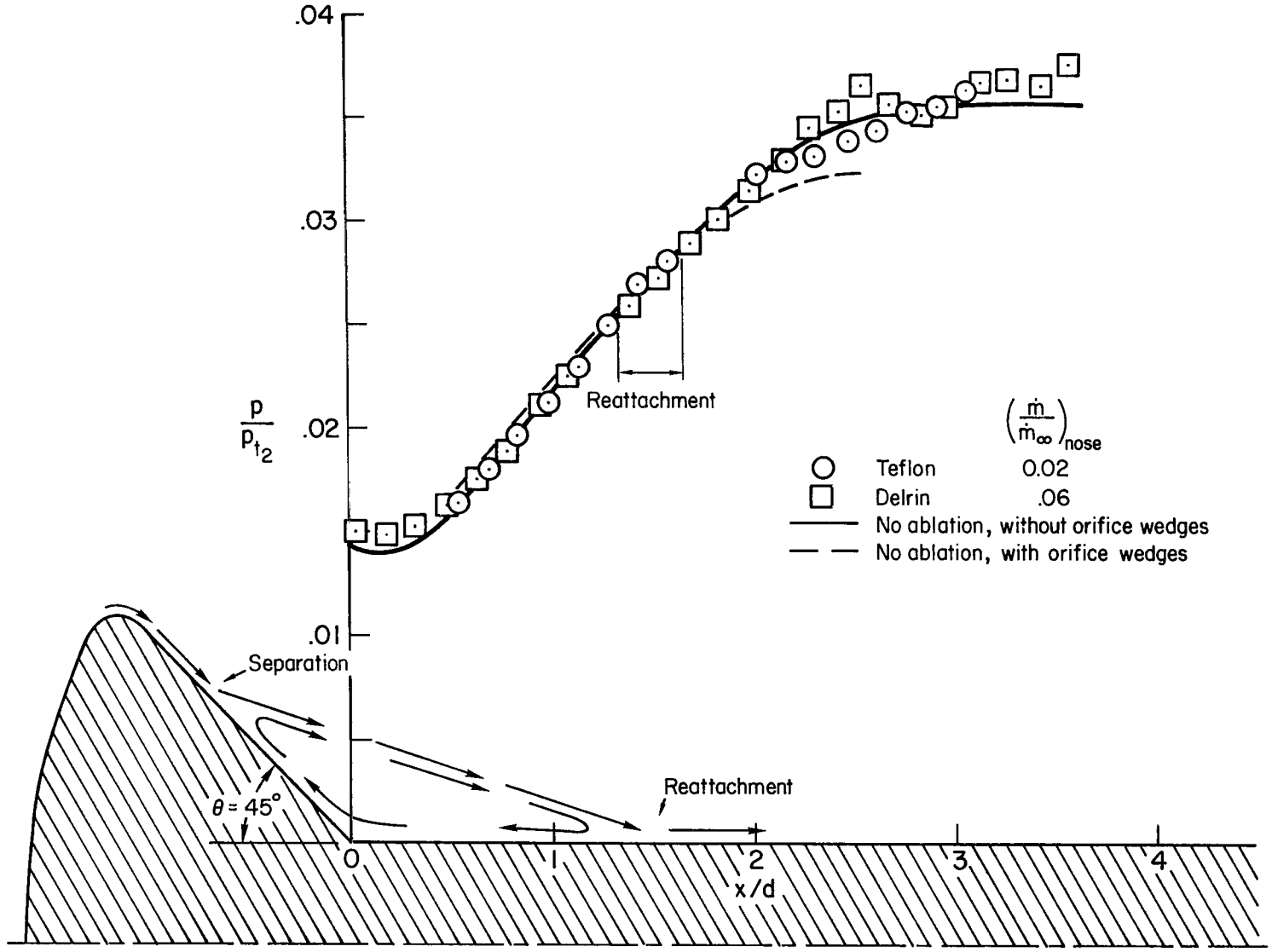

(c) $\theta = 45°$

Figure 12.- Concluded.

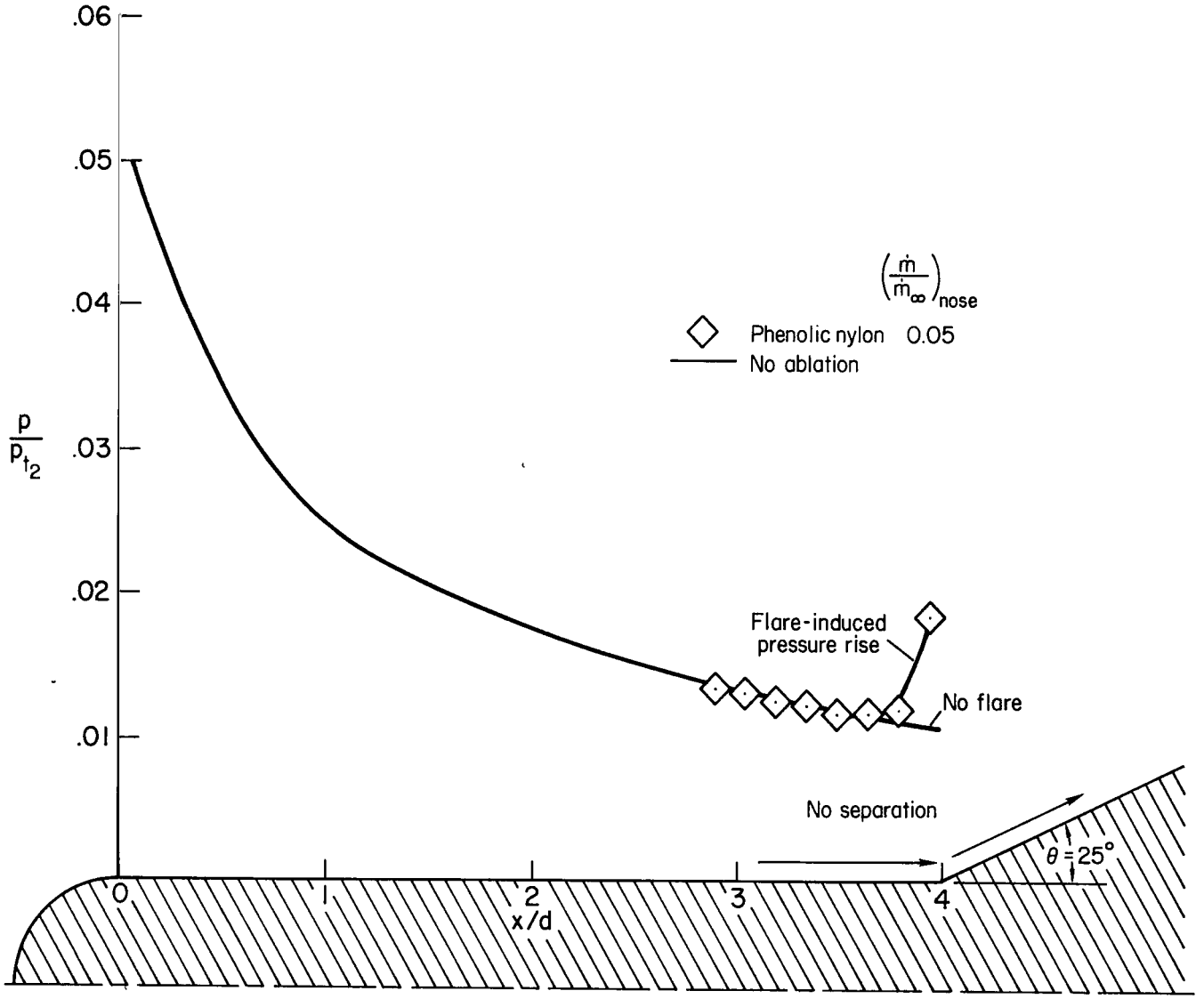

(a) $\theta = 25°$

Figure 13.- Ablation effects for the hemisphere-cylinder flare; $Re_{\infty,d} = 9000$.

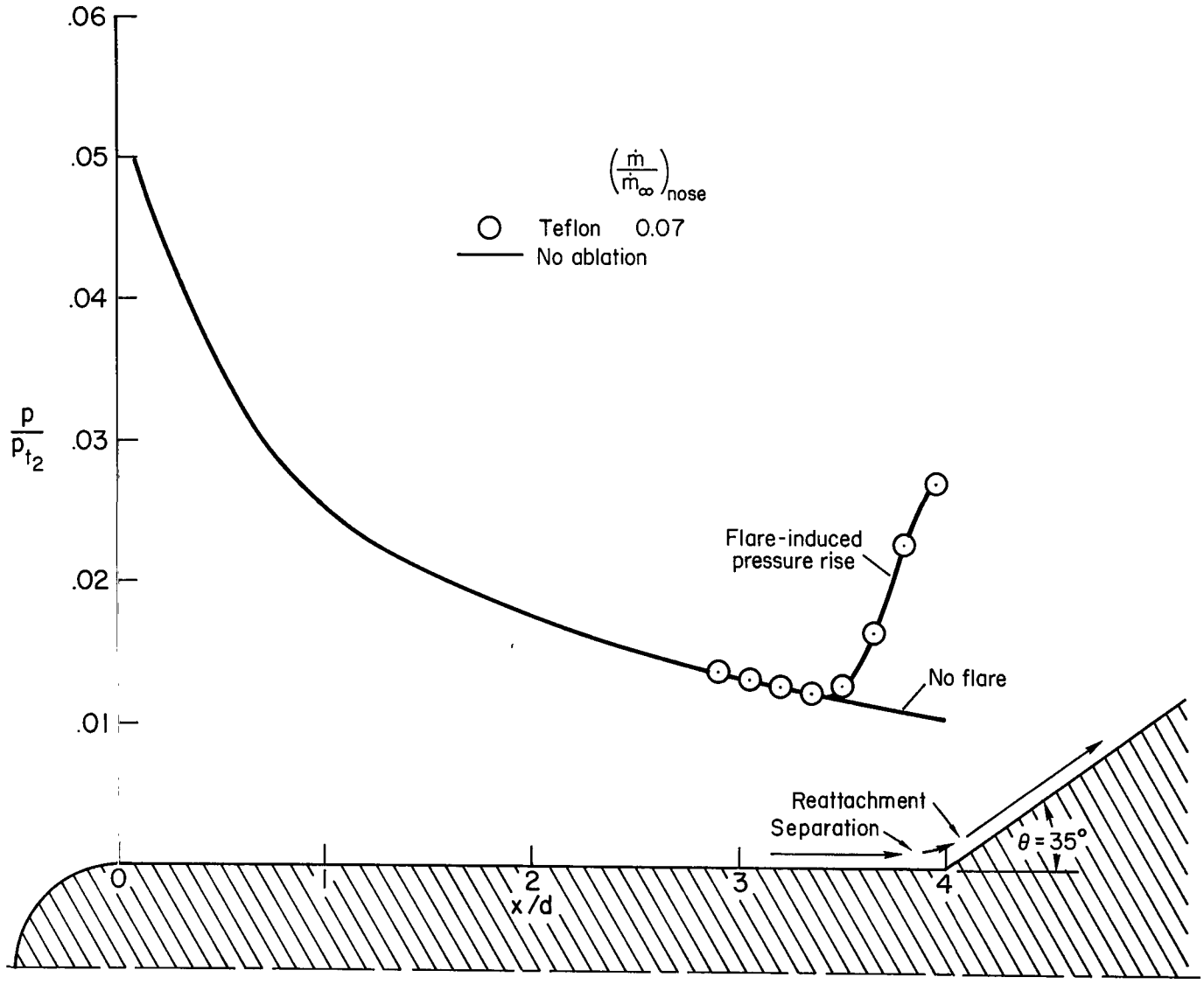

(b) $\theta = 35^{\circ}$

Figure 13.- Continued.

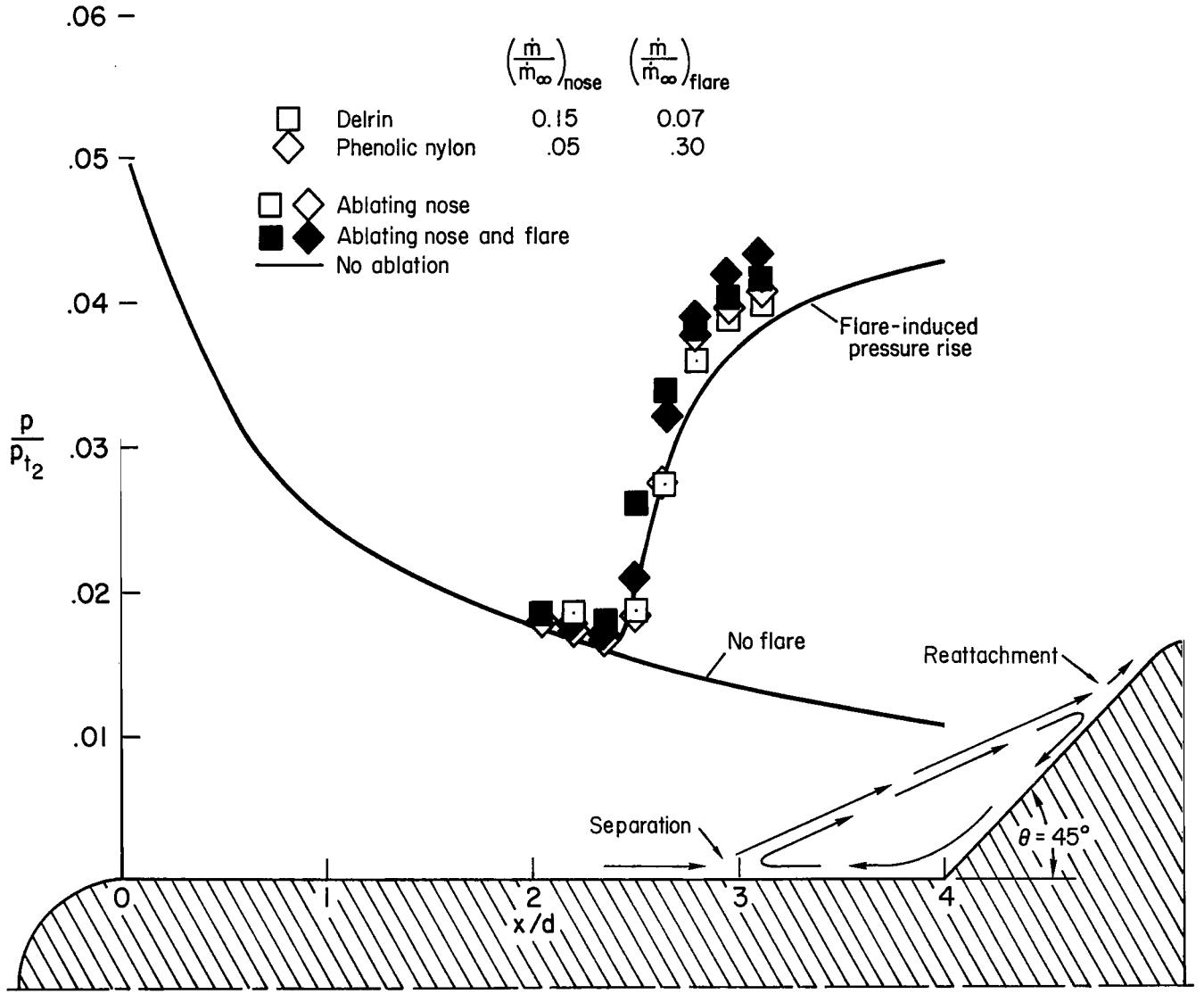

(c) $\theta = 45°$

Figure 13.- Continued.

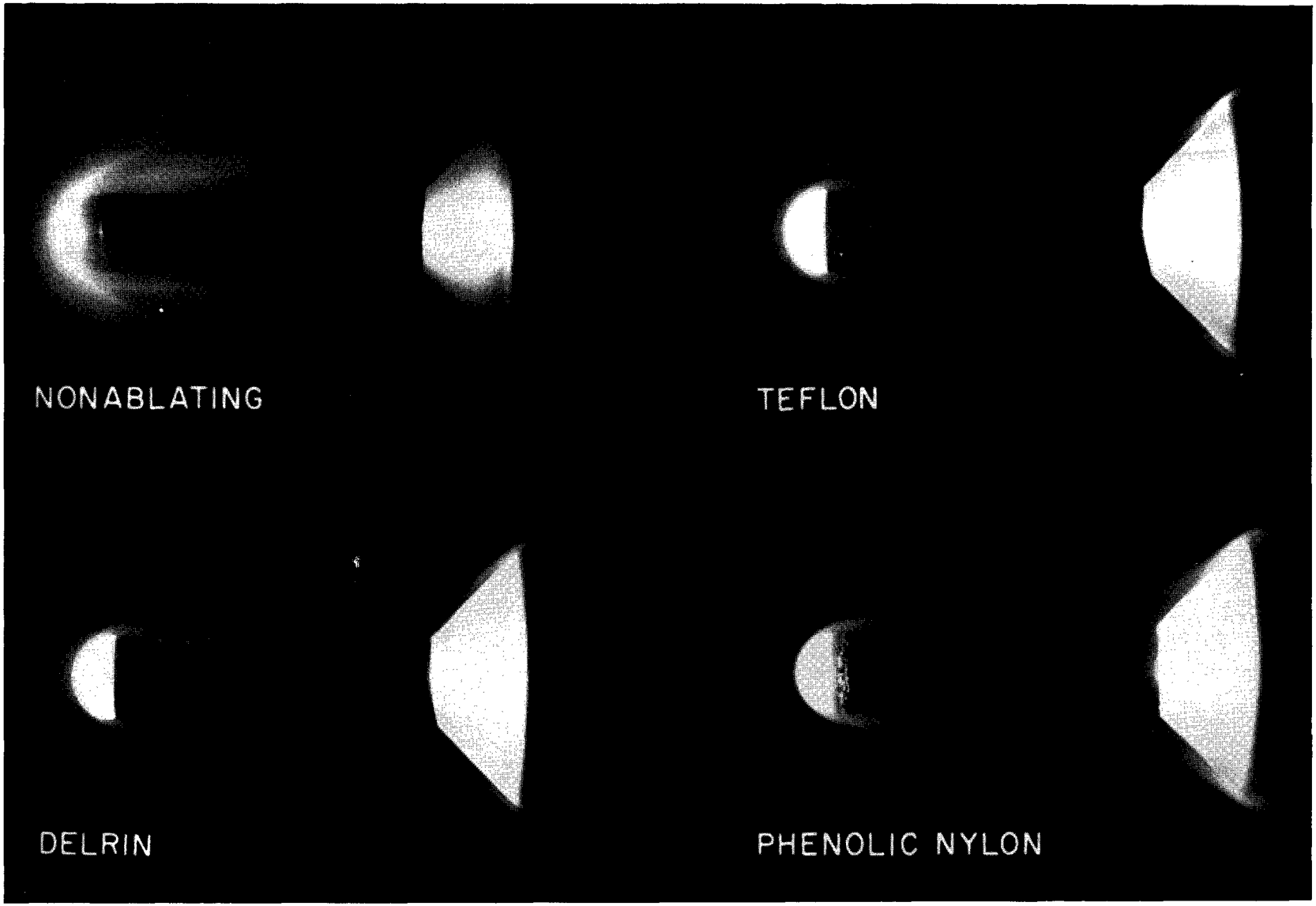

(d) $\theta = 45^{\circ}$

Figure 13.- Continued.

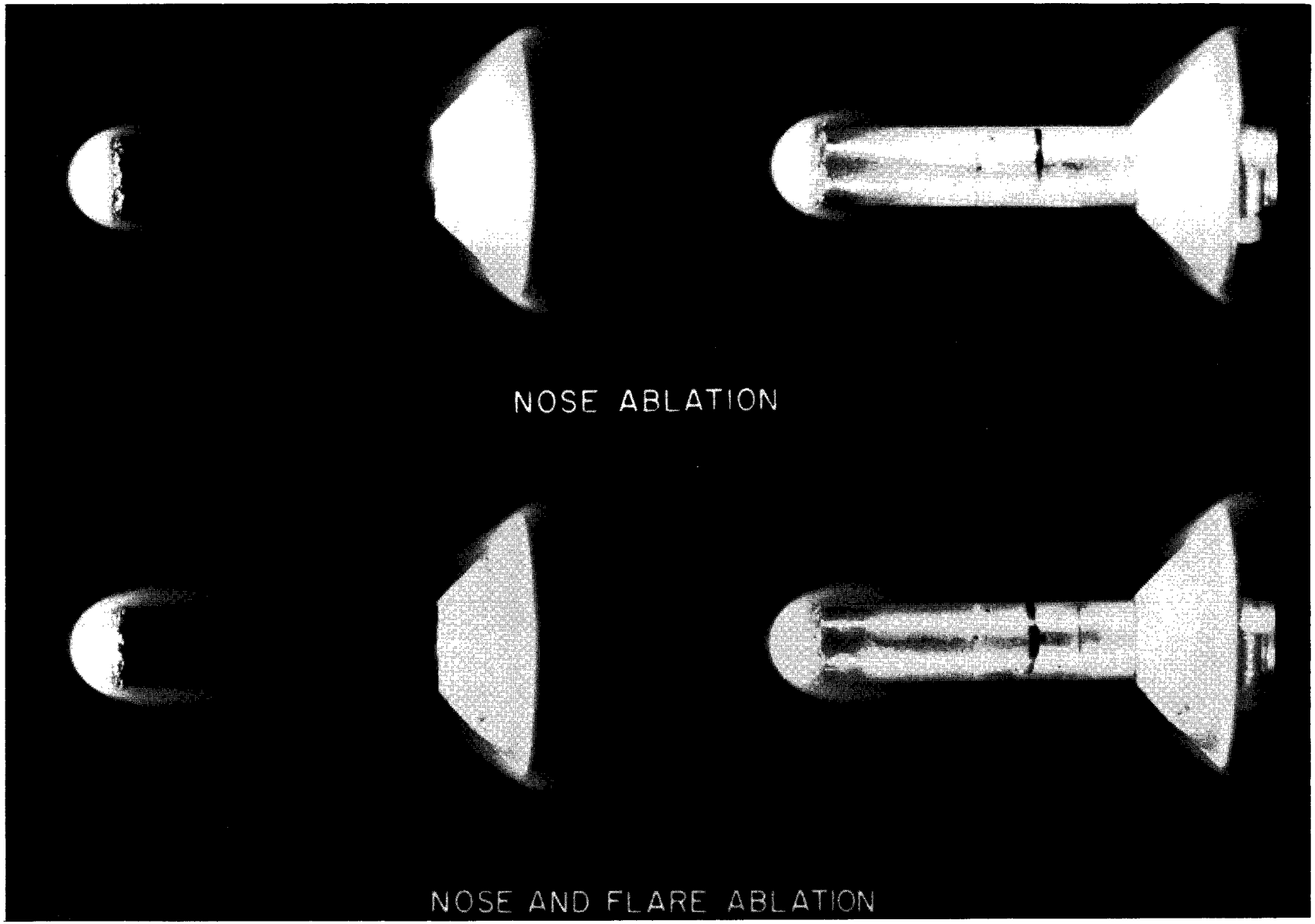

(e) $\theta = 45^{\circ}$

Figure 13.- Concluded.

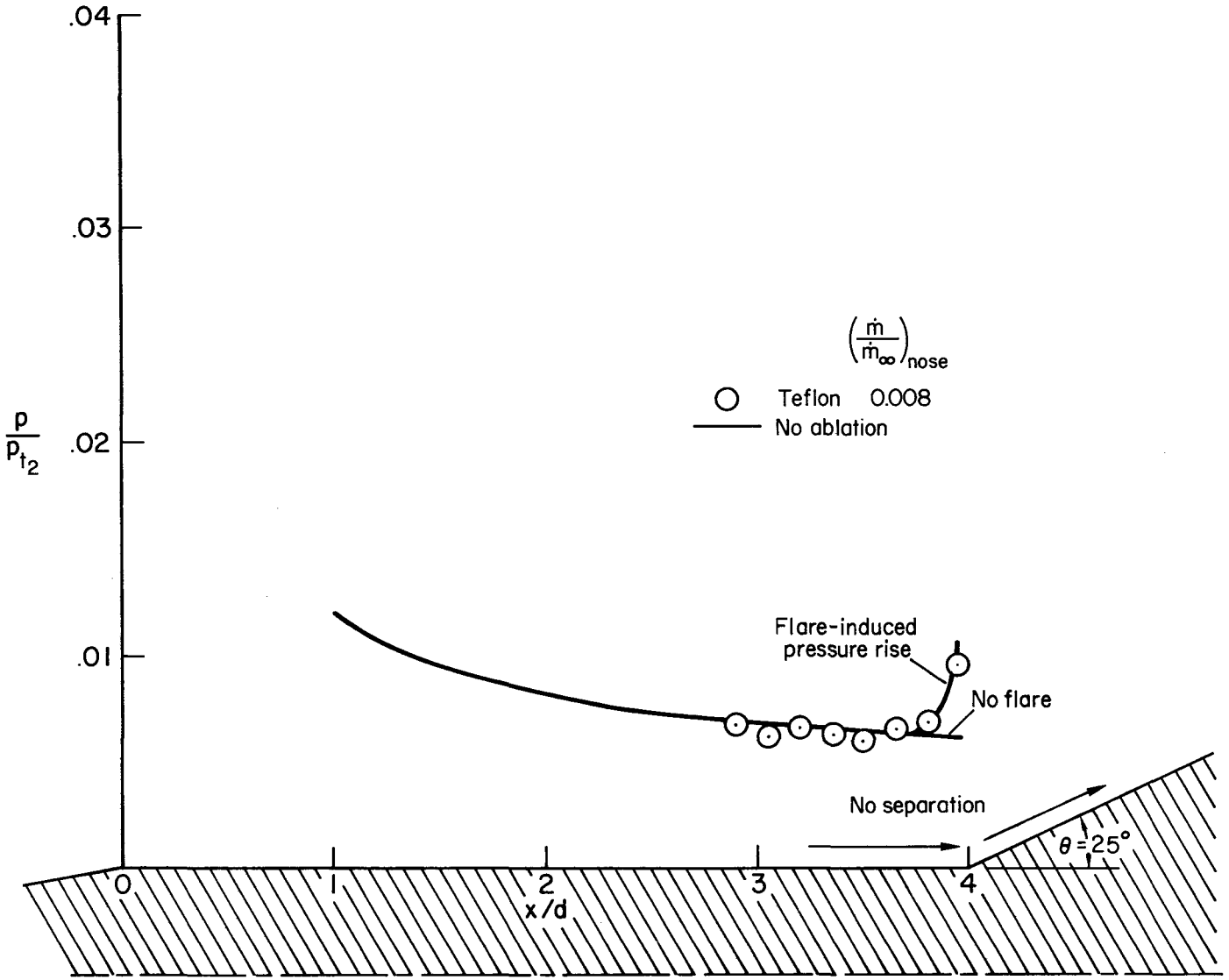

Figure 14.- Ablation effects for the cone-cylinder flare; $Re_{\infty,d}$ = 9000; θ = 25°.

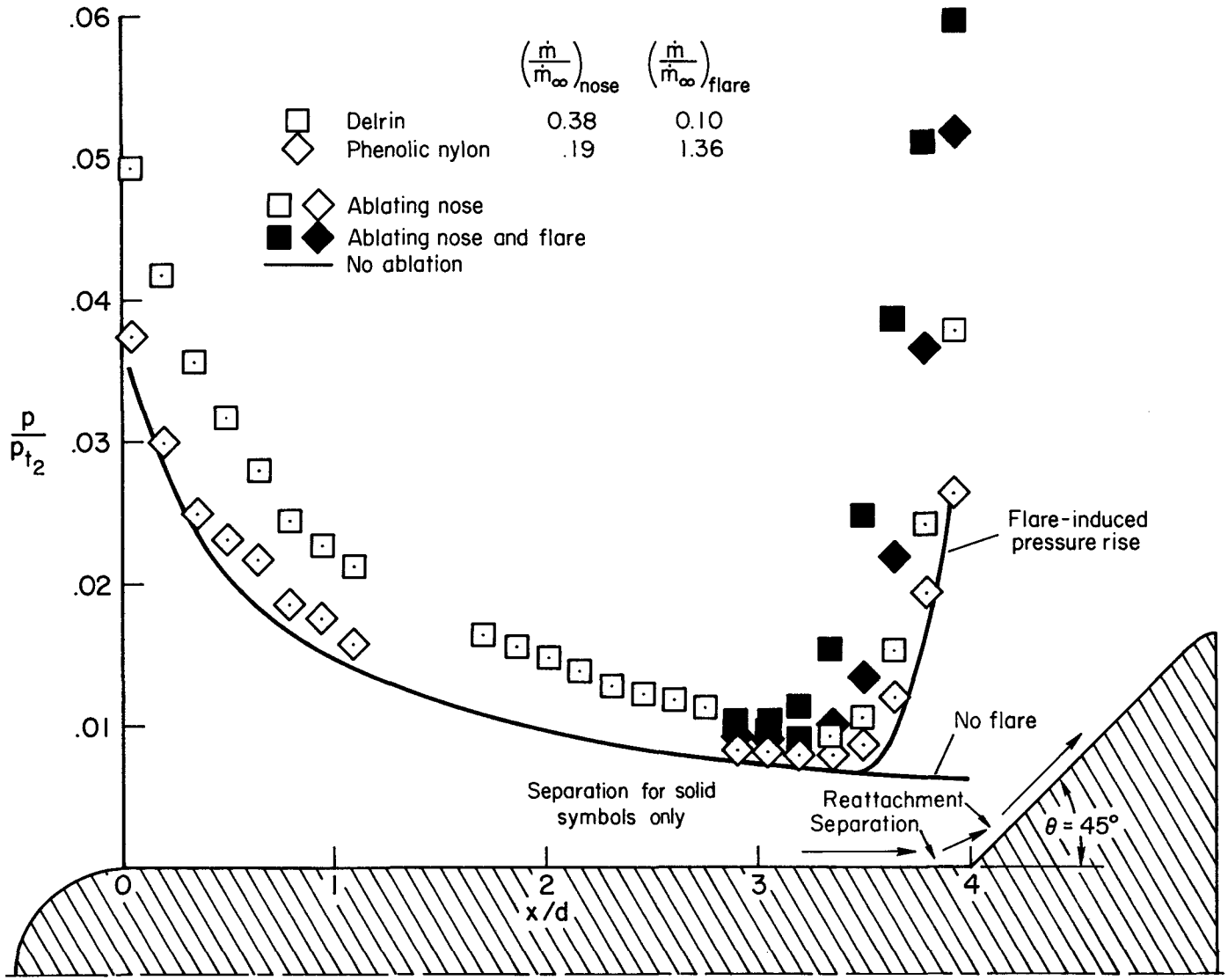

(a) $\theta = 45^{\circ}$

Figure 15.- Ablation effects for the hemisphere-cylinder flare; $Re_{\infty,d} = 1000$.

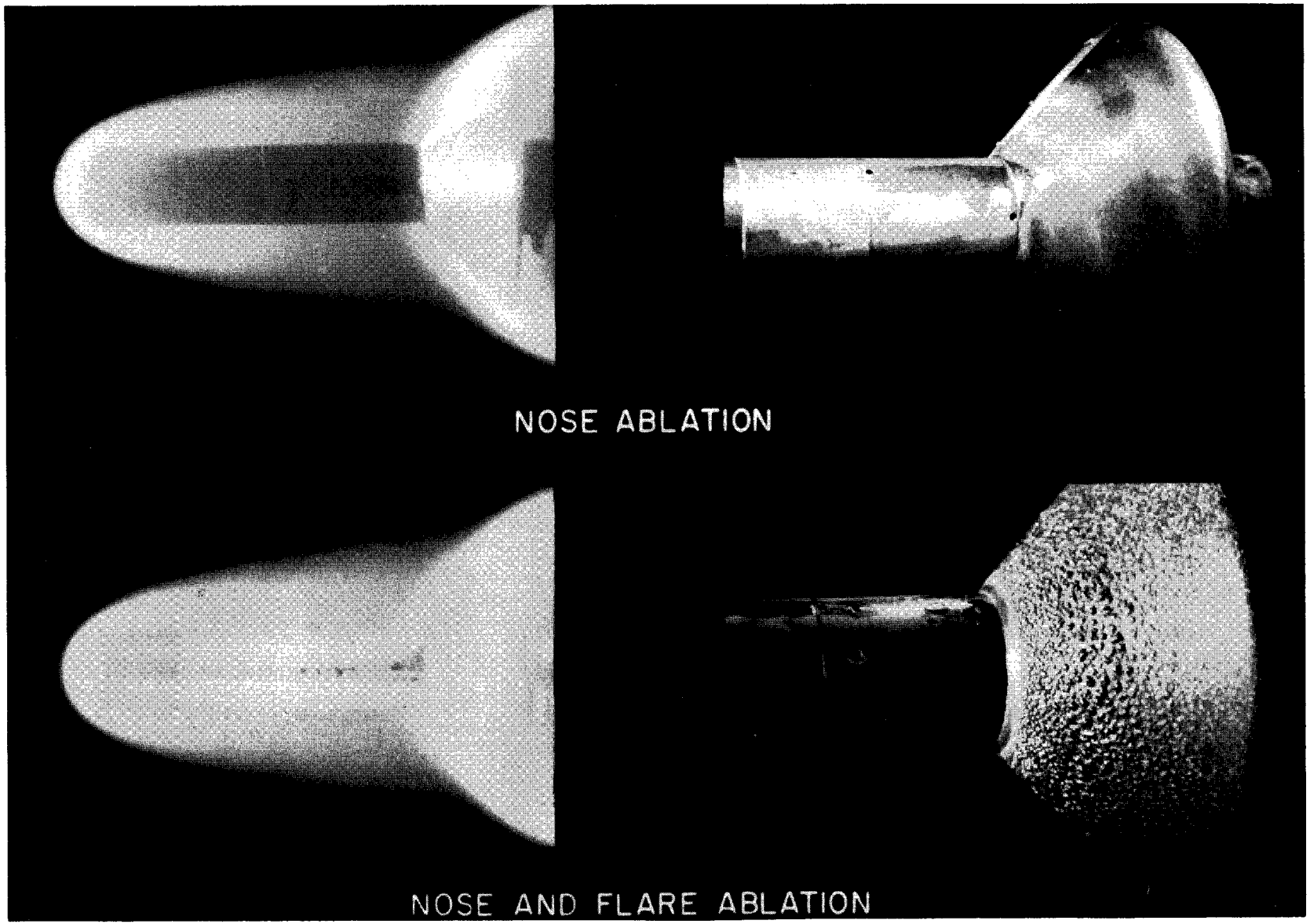

(b) $\theta = 45^{\circ}$

Figure 15.- Concluded.

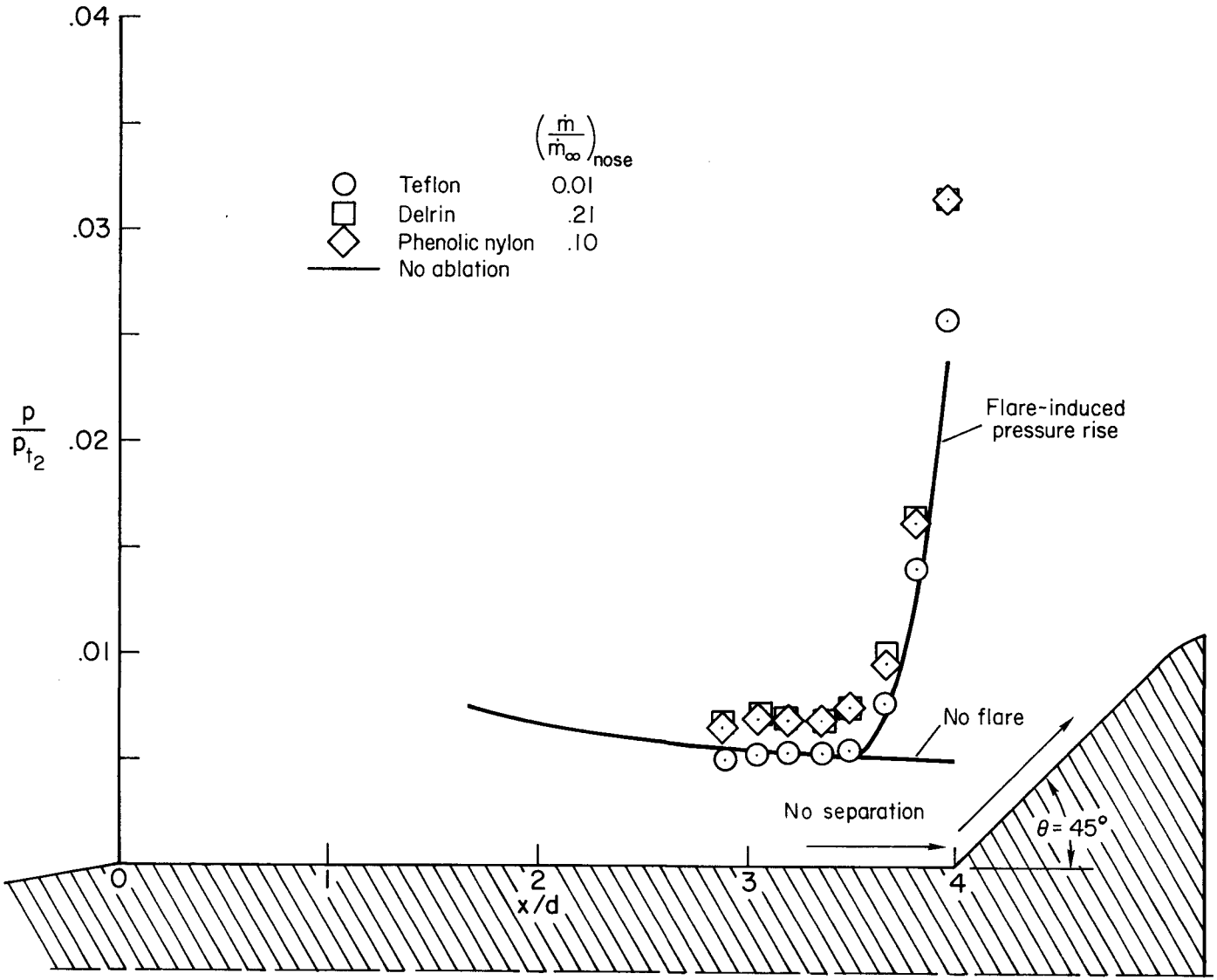

Figure 16.- Ablation effects for the cone-cylinder flare; $Re_{\infty,d}$ = 1000.

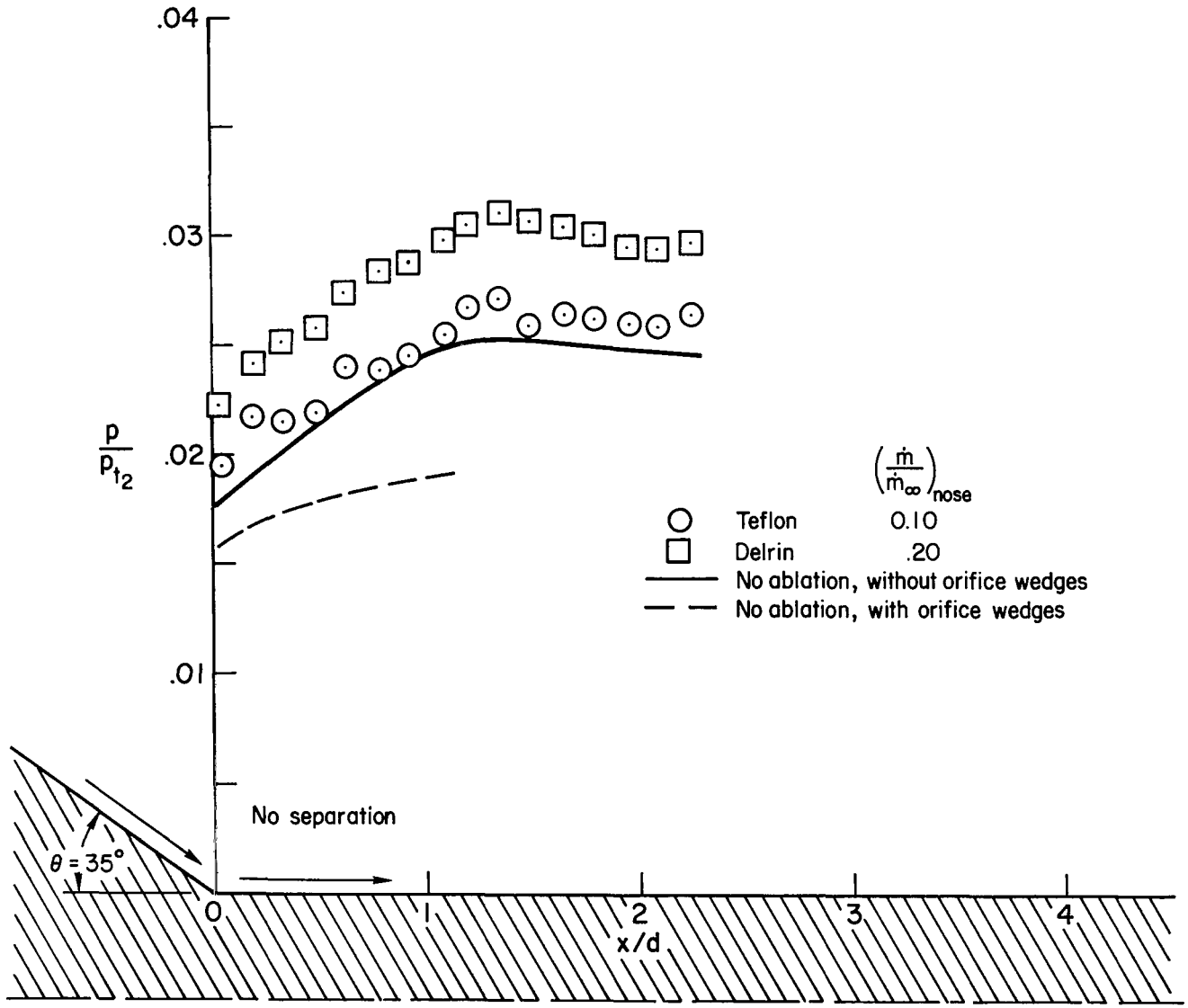

(a) $\theta = 35^{\circ}$

Figure 17.- Ablation effects for the base-flow model; $Re_{\infty,D} = 3200$.

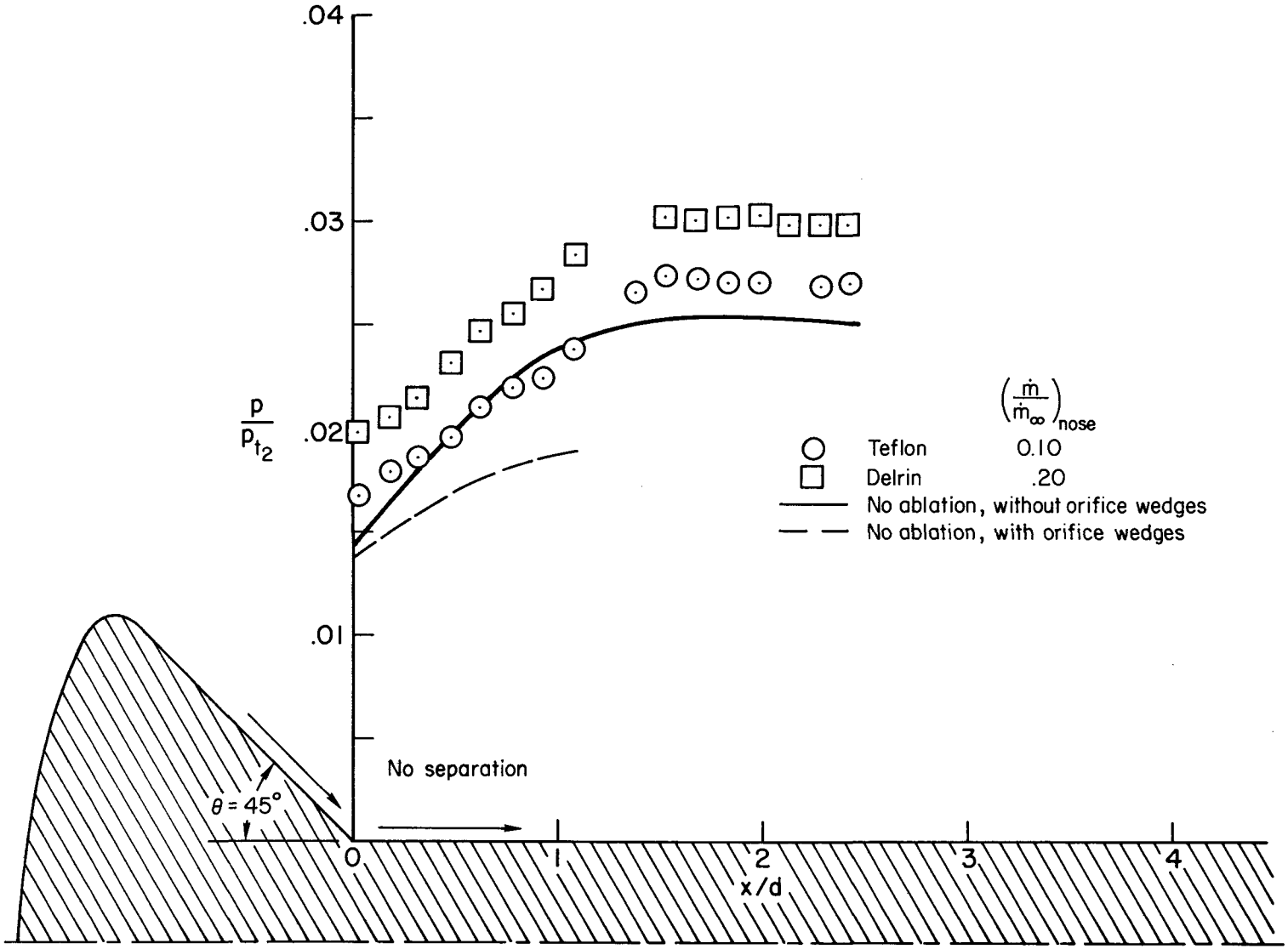

(b) $\theta = 45°$

Figure 17.- Concluded.

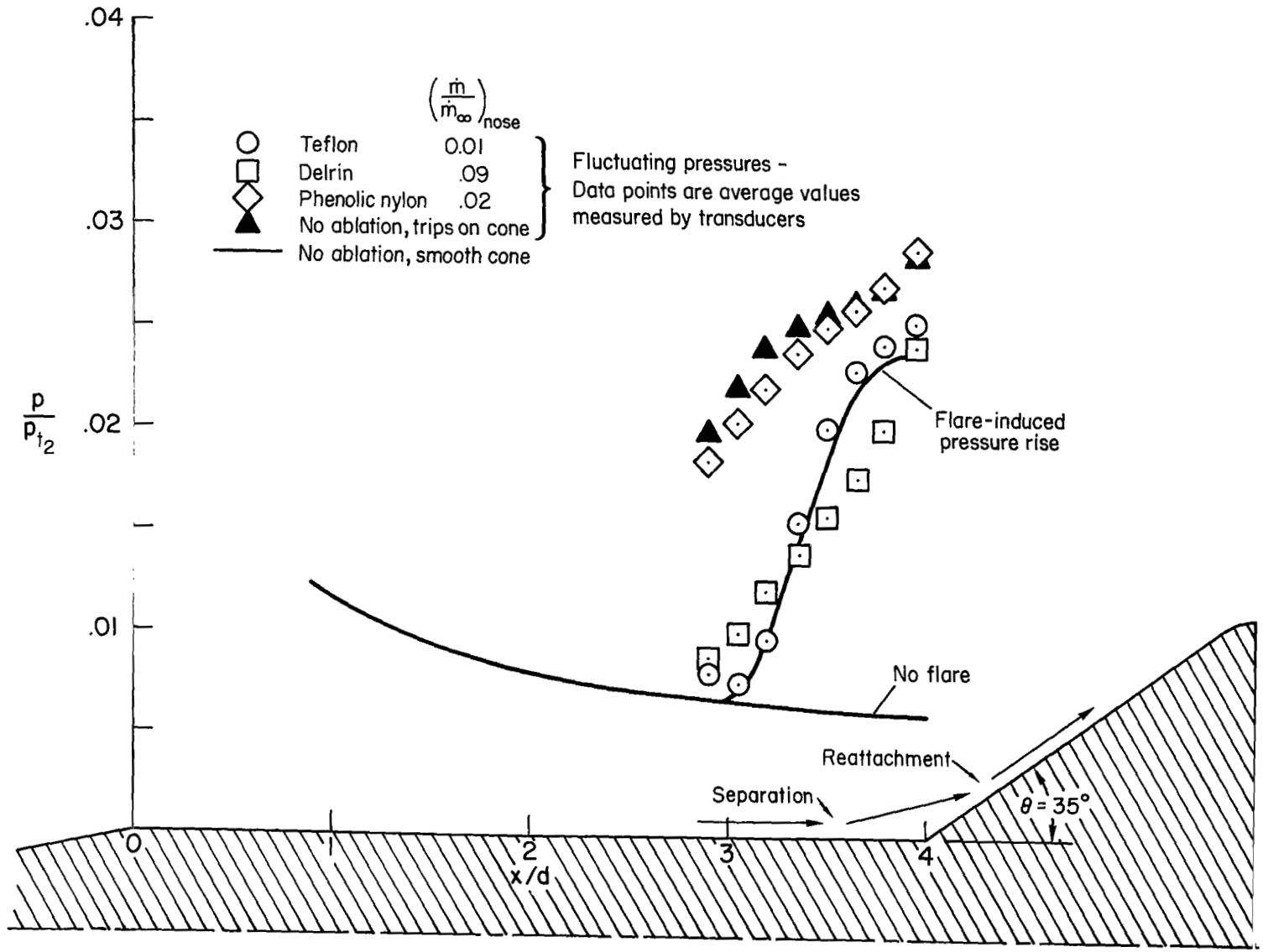

(a) $\theta = 35^\circ$

Figure 18.- Ablation effects for the cone-cylinder flare; $Re_{\infty,d} = 9000$.

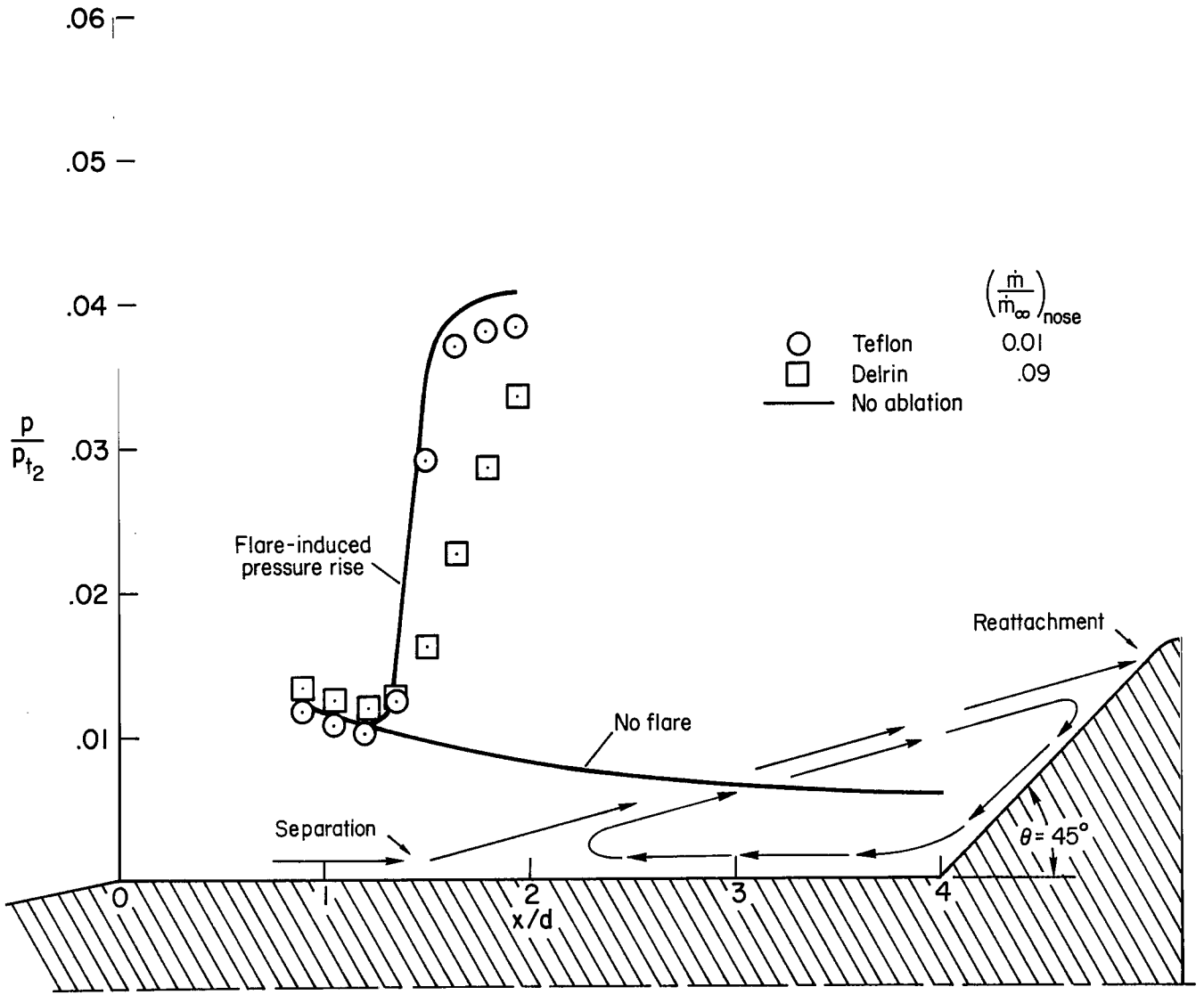

(b) $\theta = 45^\circ$

Figure 18.- Concluded.

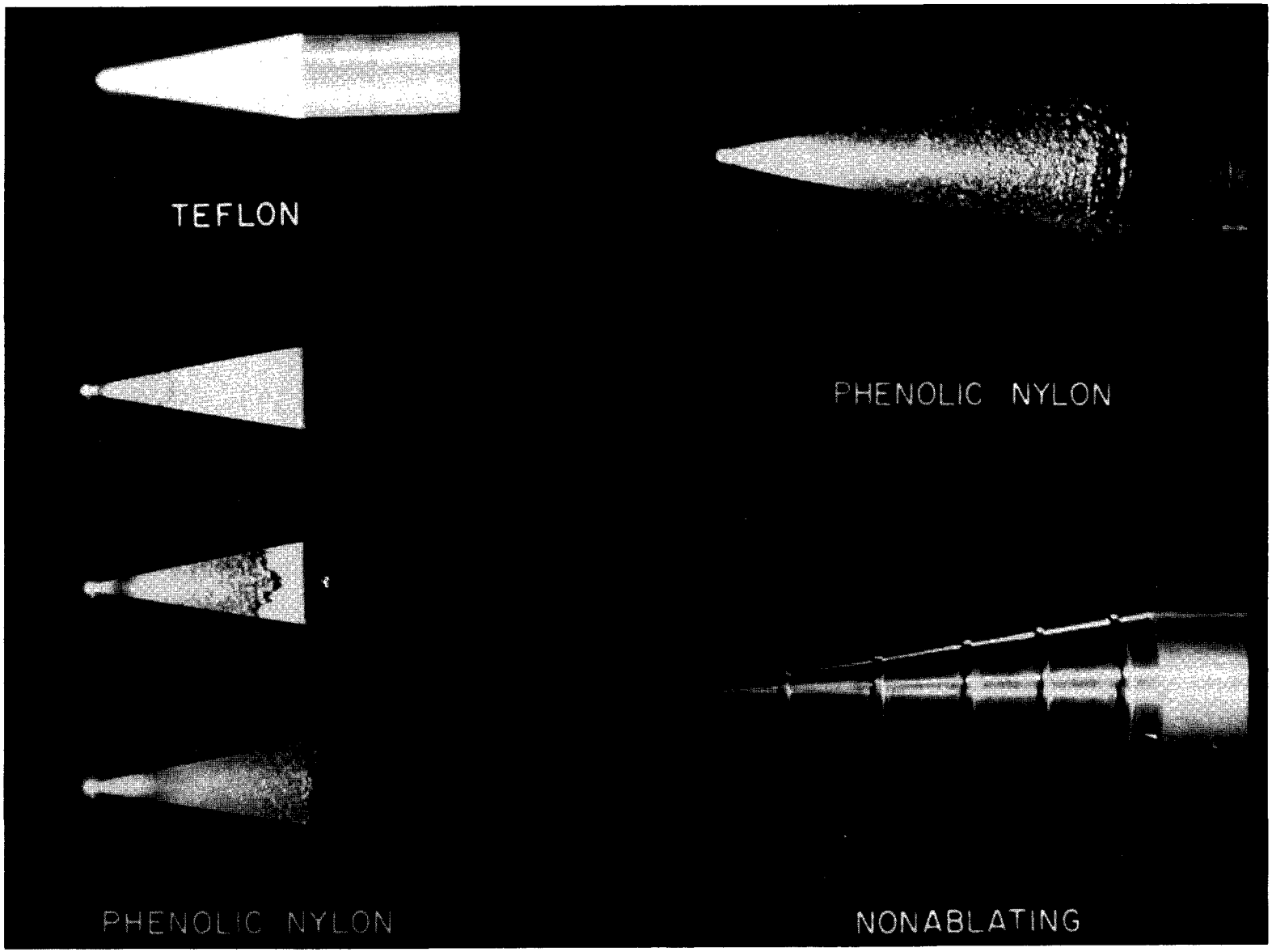

Figure 19.- Comparison of surface roughness on some of the conical noses.

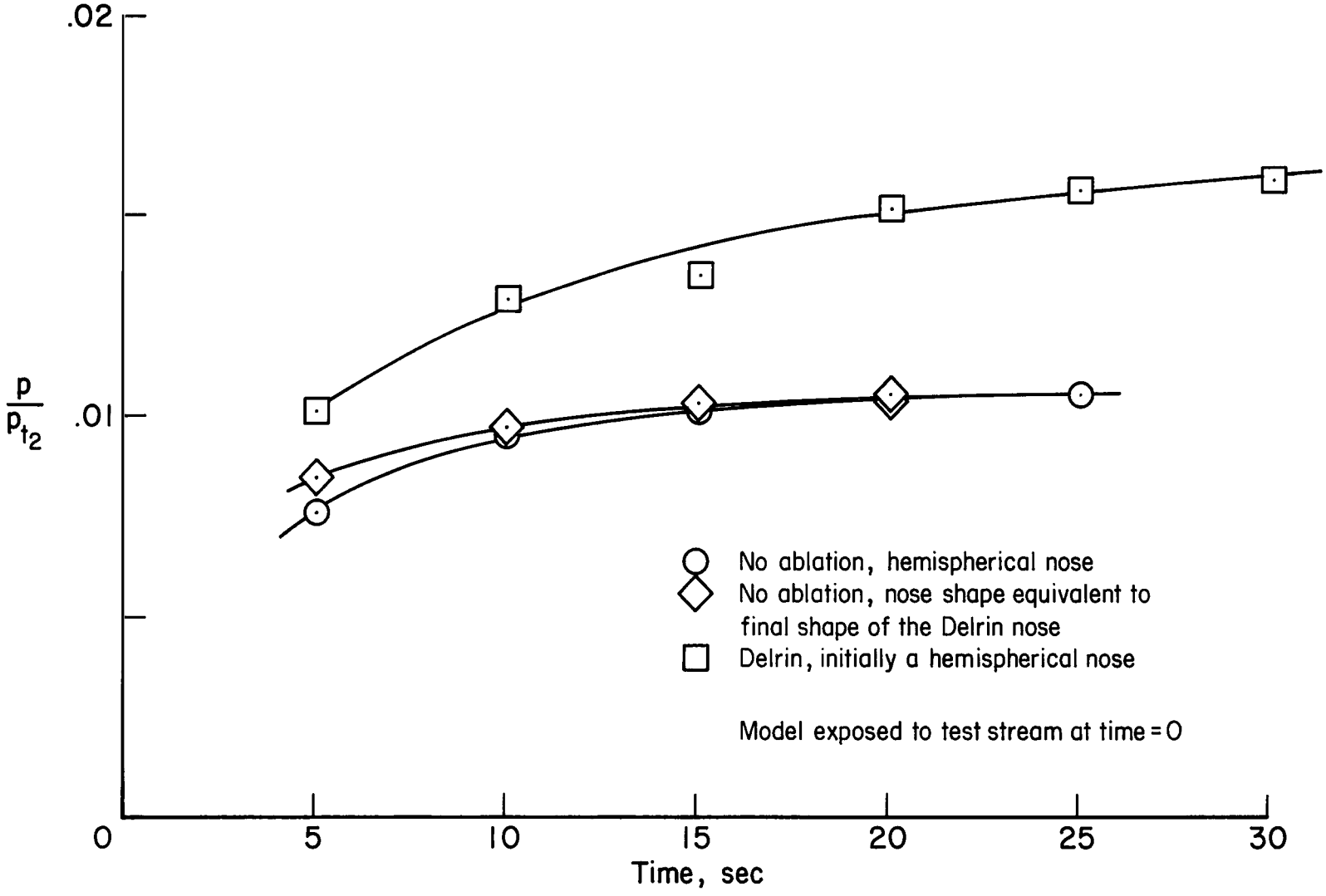

Figure 20.- Example of the time history of surface pressure on the hemisphere-cylinder model at low Reynolds number; x/d = 1.71.

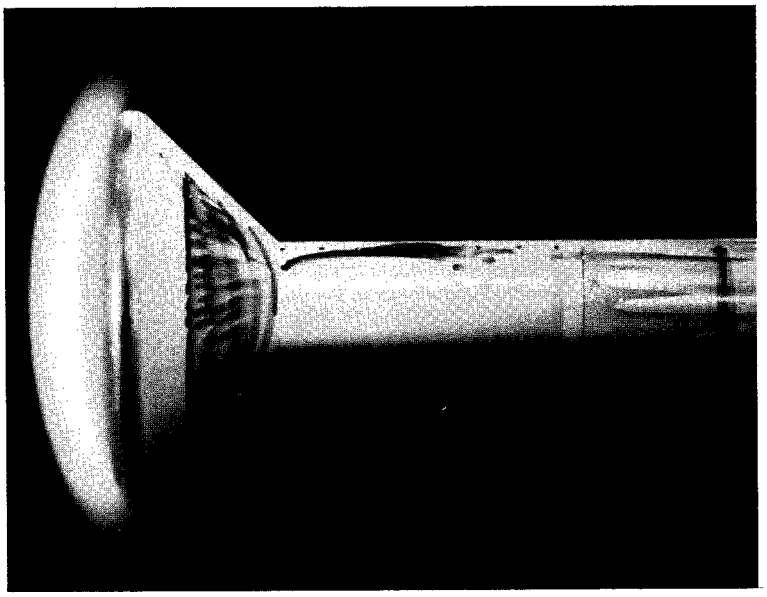

Cylinder diameter = 3.81 cm

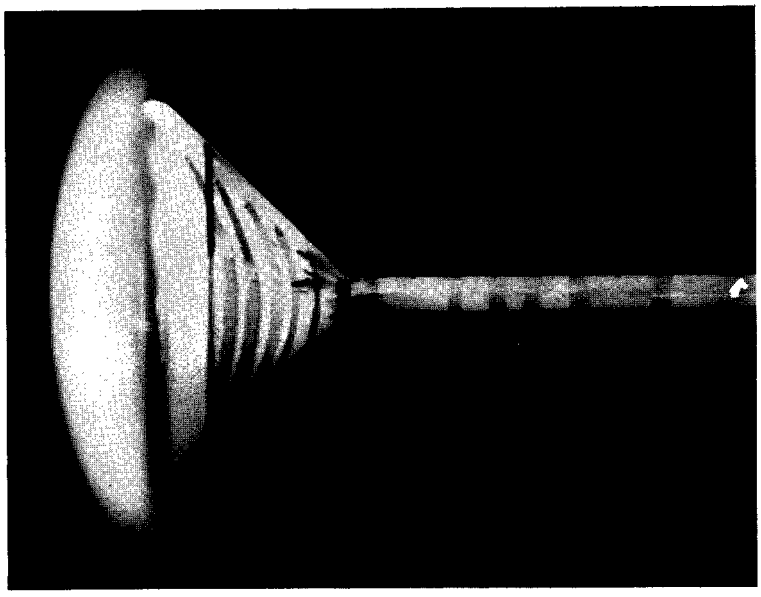

Cylinder diameter = 1.27 cm

(a) Photographs of oil flow.

Figure 21.- Effect of support diameter on the extent of separation on the base model; $\theta = 45^{\circ}$; $Re_{\infty,D} = 29{,}000$.

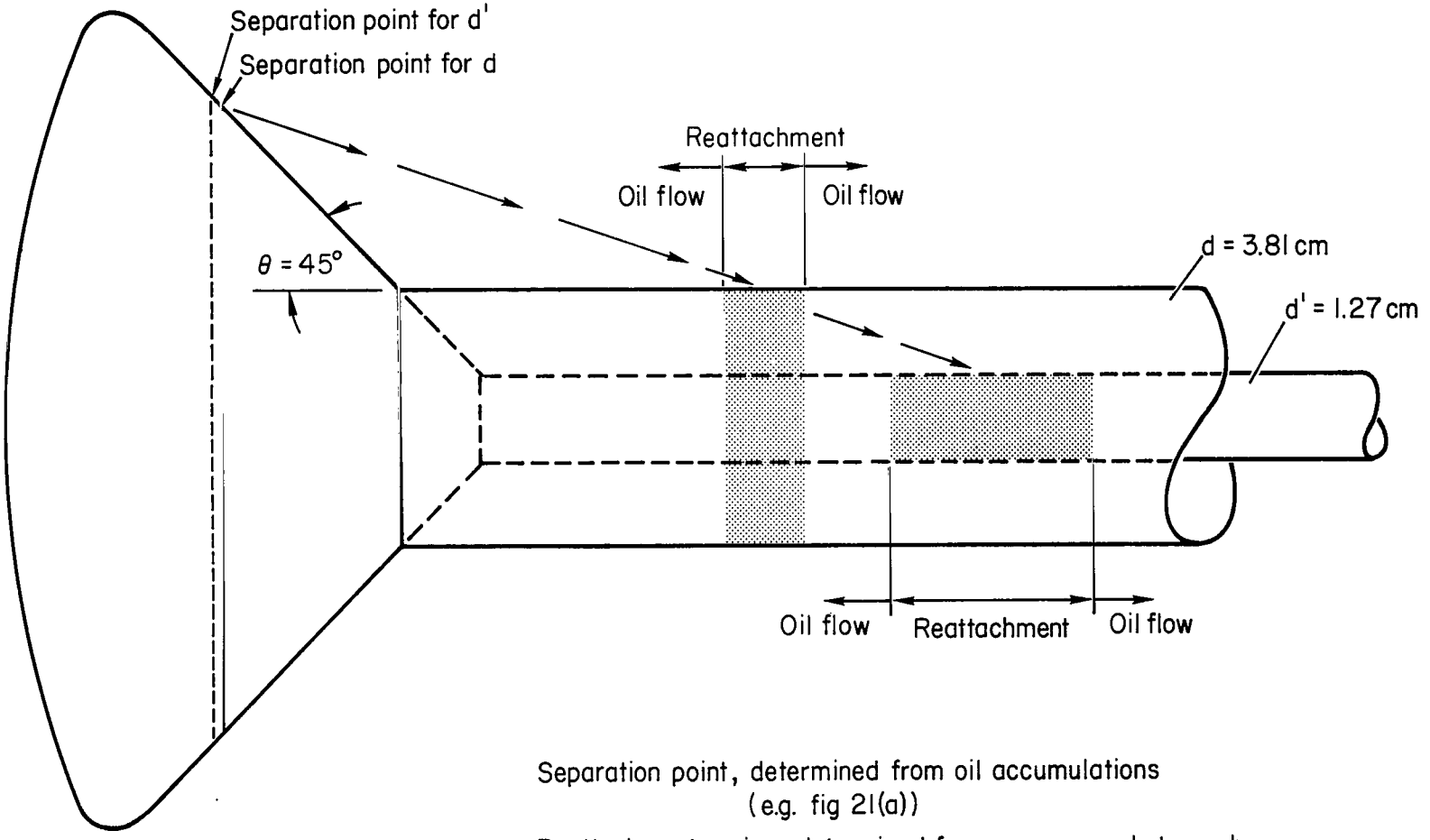

(b) Size and shape of the separated regions.

Figure 21.- Concluded.

"The aeronautical and space activities of the United States shall be conducted so as to contribute . . . to the expansion of human knowledge of phenomena in the atmosphere and space. The Administration shall provide for the widest practicable and appropriate dissemination of information concerning its activities and the results thereof."

—NATIONAL AERONAUTICS AND SPACE ACT OF 1958

NASA SCIENTIFIC AND TECHNICAL PUBLICATIONS

TECHNICAL REPORTS: Scientific and technical information considered important, complete, and a lasting contribution to existing knowledge.

TECHNICAL NOTES: Information less broad in scope but nevertheless of importance as a contribution to existing knowledge.

TECHNICAL MEMORANDUMS: Information receiving limited distribution because of preliminary data, security classification, or other reasons.

CONTRACTOR REPORTS: Scientific and technical information generated under a NASA contract or grant and considered an important contribution to existing knowledge.

TECHNICAL TRANSLATIONS: Information published in a foreign language considered to merit NASA distribution in English.

SPECIAL PUBLICATIONS: Information derived from or of value to NASA activities. Publications include conference proceedings, monographs, data compilations, handbooks, sourcebooks, and special bibliographies.

TECHNOLOGY UTILIZATION PUBLICATIONS: Information on technology used by NASA that may be of particular interest in commercial and other non-aerospace applications. Publications include Tech Briefs, Technology Utilization Reports and Notes, and Technology Surveys.

Details on the availability of these publications may be obtained from:

SCIENTIFIC AND TECHNICAL INFORMATION DIVISION

NATIONAL AERONAUTICS AND SPACE ADMINISTRATION

Washington, D.C. 20546